"ESTIMATION OF DYNAMIC AND LIQUEFACTION PROPERTIES BY SHEAR WAVE VELOCITY"

By

Suman Gautam

A
DISSERTATION
(COURSE NO. GEO 639)

SUBMITTED

TO

THE CENTRAL DEPARTMENT OF GEOLOGY

INSTITUTE OF SCIENCE AND TECHNOLOGY

TRIBHUVAN UNIVERSITY

KATHMANDU, NEPAL

IN PARTIAL FULFILMENT OF THE REQUIREMENTS FOR

THE MASTER'S DEGREE OF SCIENCE IN GEOLOGY

February 10, 2009 (Magh 26, 2065)

Date: 13 April, 2009

31 Chaitra , 2065

Letter of Recommendation

I certify that Mr. Suman Gautam has worked satisfactorily under my supervision and that the dissertation entitled "**ESTIMATION OF DYNAMIC AND LIQUEFACTION PROPERTIES BY SHEAR WAVE VELOCITY"** embodies the candidate's own research work and I, hereby, recommend the dissertation for approval by the academic board of the faculty.

_____

Surendra Raj Pant

(Supervisor)

Lecturer

Central Department of Geology

Tribhuvan University

Kirtipur

Date: 13 April, 2009

31 Chaitra , 2065

THESIS APPROVAL

The dissertation entitled, "**ESTIMATION OF DYNAMIC AND LIQUEFACTION PROPERTIES BY SHEAR WAVE VELOCITY,"** presented by Mr. Suman Gautam has been accepted as partial fulfillment of the requirement for the Master's Degree of Science in Geology by the thesis committee and the department.

COMMITTEE APPROVAL

_____

Supervisor
Surendra Raj Pant
Lecturer
Central Department of Geology
Tribhuvan University

_____

External Examiner

DEPARTMENTAL APPROVAL

_____

Dr. Megh Raj Dhital
Head
Central Department of Geology
Tribhuvan University

Acknowledgement

First and foremost, I would like to express my gratitude to my Supervisor, Surendra Raj Pant for providing me with such an interesting research opportunity and also providing me his proper guidance for the completion of my thesis.

Secondly, I would like to thank my senior colleagues Mr. Rama Mohan Pokhrel and Mr. Anil Kumar Chaudhary who without hesitatingly provided me with their useful instructions and ideas during data analysis and interpretation phase. Without their support, the thesis completion would have become rather difficult. I am very grateful to senior colleagues as well as staffs of ITECO CMAT GEOTECH SERVICES P. LTD, Mr. Sattyam Poudel and Ajay Raj Adhikari who continuously assisted me during data acquisition phase. Mr. Shiva Basnet also deserves special thanks for being available during wonderful discussion about the topics as well as providing me essential articles.

I am very grateful to my cluster friends, Rajendra Neupane, Surya Limbu, Kanchan Chaulagai, Pankaj Devkota, Shrawan Khanal, Namraj Bhattarai, and Kumar Khadka. Their technical support during documentation is always unforgettable.

Lastly, I am very grateful to my parents, specially my Mom, brothers and Aunts, for their quality endurance and continuous financial support.

Suman Gautam
February, 2008

Abstract

The analysis of foundation vibrations and geotechnical earthquake engineering problems in civil engineering requires characterization of dynamic soil properties using geophysical methods. Dynamic structural analysis of the superstructures also requires knowledge of the dynamic response of the soil-structure, which in turn relies on dynamic soil properties. Geophysical methods are often used to characterize the dynamic soil properties of the subsurface. This method requires a borehole through which a sensing probe is lowered at known level. Source near the borehole is generated artificially with the help of wooden plank and hammer. The seismogram obtained from computer aided system is used to determine shear wave velocity and compressive wave velocity which is further used to calculate dynamic parameters such as Poisson's ratio, dynamic shear modulus, dynamic elastic modulus and predominant period etc. Ground water table is very close to ground surface and the soil is mainly fine to coarse sand with some intermittent layers of cohesive soils meaning that the soil is very liable to liquefaction. Liquefaction resistance is assessed in terms of cyclic stress ratio and in terms of factor of safety both of which show that the liquefaction potential of the site is very high mainly near shallow depth less than 10m.

Key Words: *Shear Wave Velocity, Predominant Period, Cyclic Stress Ratio, Cyclic Resistance Ratio, Factor of Safety, Soil Liquefaction*

Table of Contents

List of Tables

List of Figures

Page

List of Annexure

CHAPTER ONE

INTRODUCTION

1.1Background

Natural disasters such as earthquakes, floods, tornados and drought etc are unavoidable, but their effects can be mitigated to some extent by disaster prevention systems. Earthquakes are the most destructive of the various geological hazards. During the twentieth century, well over 1,000 fatal earthquakes were recorded with a cumulative loss of life estimated at 1.5 – 2.0 million people (Pomonis, 1993).

It is important to know the local soil conditions and topography. The effect of local site conditions on the amplification of ground motions has long been recognized (Seed 1982). Depending on the subsurface characteristics, seismic waves might undergo amplification and create more severe strong ground motions at the surface. Many earthquake prone cities are settled over very susceptible areas with young deposits such as Mexico City (Seed, Romo et al. 1987), Loma Prieta (Rodriguez-Marek and Bray 1999) and Kathmandu. Having a high potential for earthquakes and a susceptible local site environment, the situation in Kathmandu might turn a hazard into a disaster in the future.

Kathmandu valley is densely populated capital city of Nepal with about 7% of the total population of the country. The number of residential houses, business complexes, schools, colleges and hospitals is increasing everyday mostly in last two decades. The Kathmandu valley is filled with soft Pleistocene sediments of fluvio-lacustrine origin, which are said to be geotechnically unpredictable. But, still there is less or almost no care to the soil foundation characteristics in construction of the private or public infrastructures. Only a few residential and public buildings are being constructed taking proper care of geotechnical characteristics of the basement soil.

1.2 Location and Accessibility

The study area lies in the Kathmandu district towards northern part near Chakrapath, in the compound of Australian Embassy. The site is easily accessible by any means of transportation. Altogether nine boreholes are made to extract geotechnical and lithological information. Out of the nine bore holes, only three boreholes were utilized for borehole geophysical test.

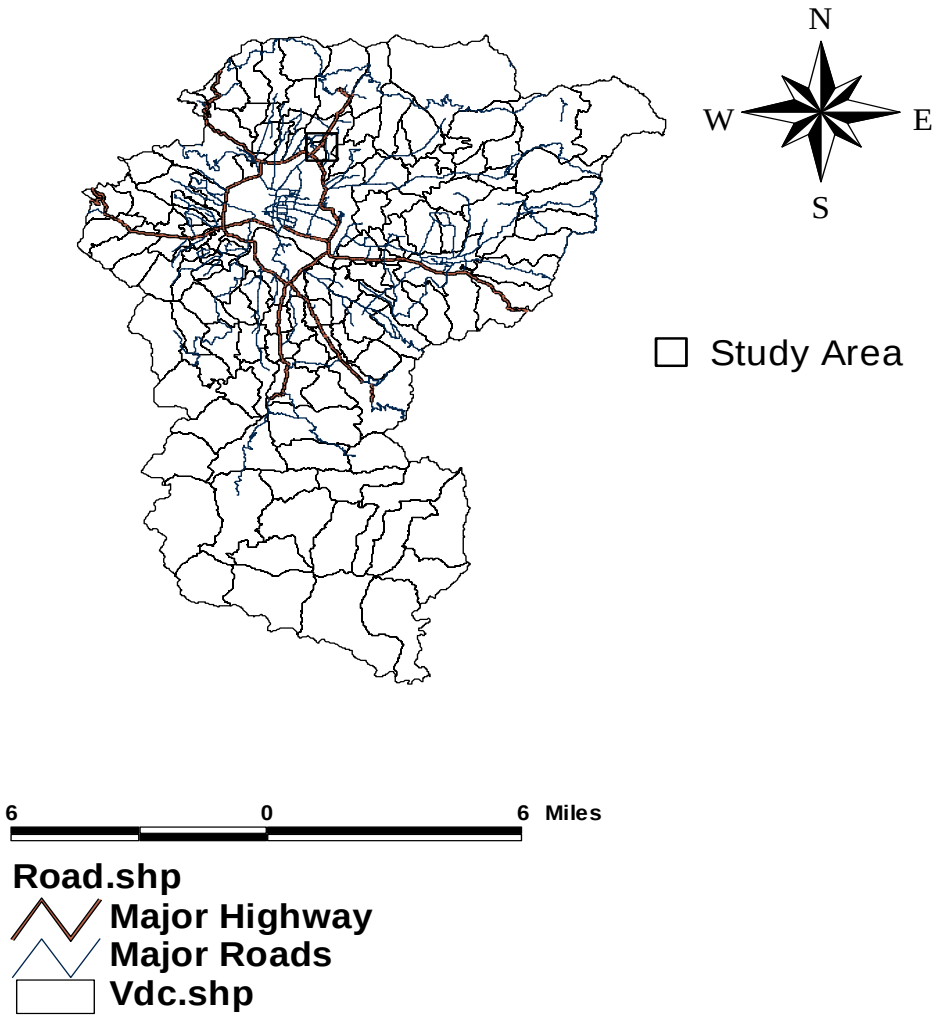

Fig. 1.1 Location Map of the Study Area

1.3 Objectives

This study is primarily focused on acquiring necessary geophysical information to calculate various dynamic properties of the soil like Young's modulus, Shear modulus, Poisson's ratio etc as well as earthquake parameters such as predominant period, peak ground acceleration etc. The objectives of the study are as follows:

- To calculate the dynamic parameters and predominant period of the ground up to depth of 30 m.
- To calculate ground amplification ratio for combination of different predominant ground periods and time periods of incoming component waves.
- To correlate shear wave velocity with other seismic and geotechnical parameters.
- To assess liquefaction potential for different layers for different values of peak ground acceleration (PGA) considering fault nearest to Kathmandu valley.
- To evaluate liquefaction resistance based on shear wave velocity.

1.4 Methodology

This dissertation is presented after thorough field study and desk study. Geophysical investigation of the site was carried out utilizing down the hole seismic technique in three of the available borehole. Geotechnical information was obtained from the ITECO-CEMAT GEOTECH SERVICES (P.) LTD. [ICGS]. The following general methodological schemes purposed and applied for the preparation of the dissertation are grouped under the following headings:

- Literature survey
- Data acquisition
- Data processing
- Data Analysis

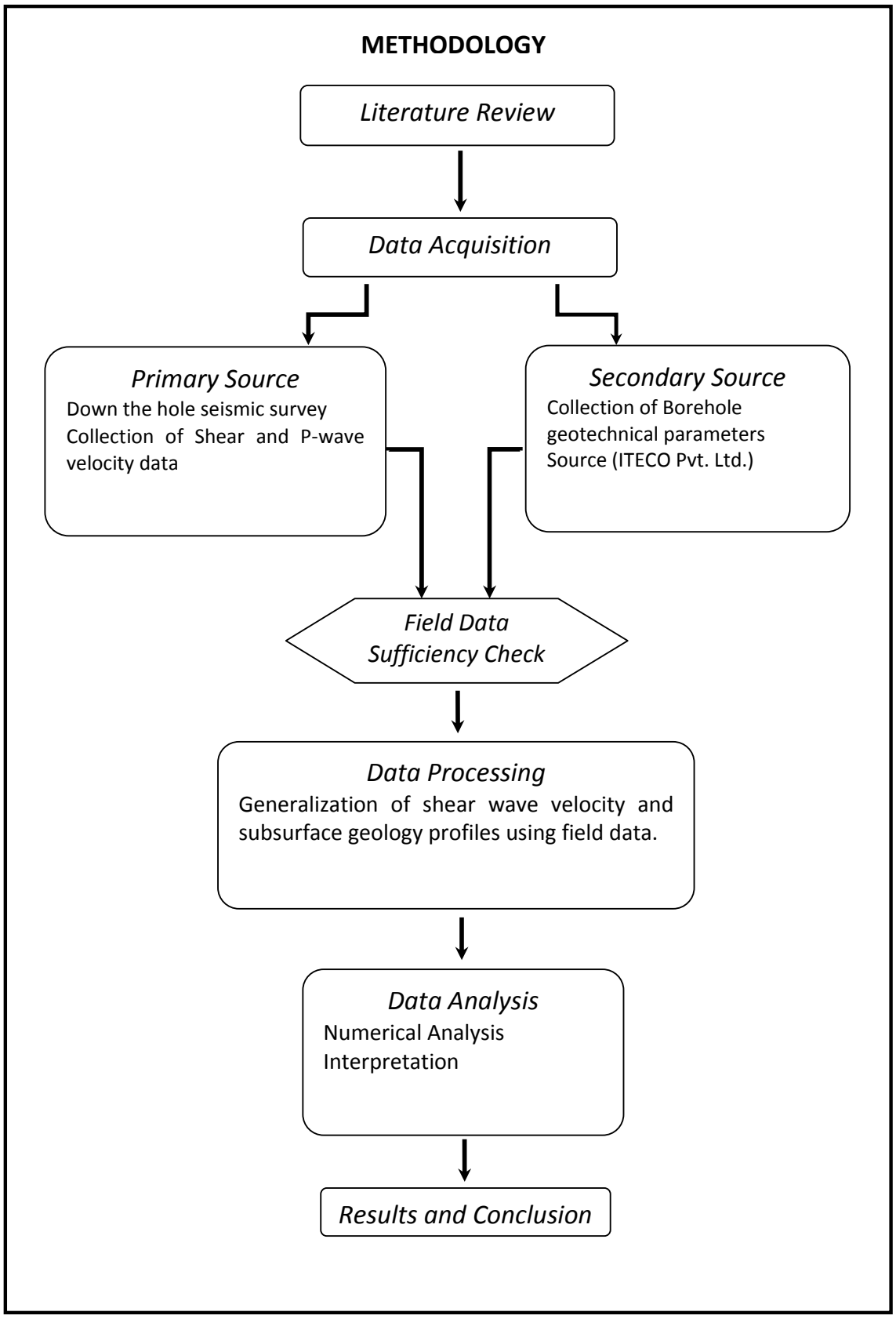

Fig. 1.2: ***Flowchart of the methodology used in the research***

1.5 Structure of the Thesis

The structure of the thesis in short explanations is as follows:

- Chapter one gives a general context of the study including the introduction, general objectives and methodology.
- Chapter two presents general overview of the geology of the Kathmandu valley.
- Chapter three presents general aspects on theory of elasticity and seismic methods.
- Chapter four outlines the field procedure employed for the acquisition of geophysical data.
- Chapter five gives the detail of data analysis and interpretation.
- Chapter six gives the details of numerical approach employed for the assessment of liquefaction resistance.
- Chapter seven gives the findings and the conclusions of the study.

CHAPTER TWO

GEOLOGY OF KATHMANDU VALLEY

2.1 INTRODUCTION

Kathmandu valley is a large intermontane basin carried above the Himalayan major detachment and it is the largest basin situated in the Lesser Himalaya of Nepal. This basin lies on the basement of crystalline rocks and Precambrian to Paleozoic metasedimentary formations which occupies the large core of the Mahabharat Synclinorium. It extends for about 30 km in the east-west direction and about 25 km in the north-south direction. The basin is filled with a very thick (more than 650m) sequence of fluvio-lacustrine sediments (Moribayashi and Maruo, 1980) that covers about 400 km^2 in area. Moribayashi and Maruo (1980) carried out the gravity survey to delineate the basement topography of the Kathmandu valley. They estimated the maximum thickness of the basin filled sediment to be about 650 m. The semi-consolidated sediments filling the basin mainly consist of mud, silts, sandy loam, fine to coarse sands, and gravel to cobble conglomerates. Within the valley, the basement rocks protrude above soft sediment in some localities as exotic outcrops.

The geology of the Kathmandu area has been investigated in detail by Stocklin and Bhattarai (1977) and Stocklin (1980).They have included all the rocks of Kathmandu area into Kathmandu Complex which is further divided into the lower Bhimphedi Goup and the conformably overlying Phulchauki Group. The Bhimphedi Group consists of relatively high-grade metamorphic rocks of pre-cambrian age. It is about 8 km thick and includes six formations: Raduwa Formation, Bhainsedobhan Marble, Kalitar Formation, Chisaspani Quartzite, Kulekhani Formation, Markhu Formation. The Phulchauki Group comprises the weakly metamorphosed sedimentary rocks of early-middle Paleozoic age. It is 5-6 km thick and is divisible in to five Formations: Tistung Formation, Sopyang Formation, Chandragiri Limestone, Chitlang Formation and Godavari Limestone.

The geology and related fields of the area have been studied by a number of workers, such as Dhoundial (1966), Yonechi (1973), Thapa (1977), Akiba

(1980), Moribayashi and Maruo (1980), Stöcklin (1980), West and Munthe (1981), Tuladhar (1982), Yamanaka (1982), Yoshida and Gautam (1988), Sah et al. (1991), Adhikari (1993), Koirala et al. (1993), Kizaki (1994), Katel et al. (1996), Sakai et al. (2001), Sakai T. et al. (2001), Gautam et al. (2001).

2.2 Pleistocene Geology

The basement of the Kathmandu valley is covered by the soft sediment of the Plio-Pleistocene age. The basin is filled by thick semi-consolidated fluvio-lacustrine sediments. The maximum depth of the basement is estimated to be a little more than 650 m from the present surface of the valley under Baneswor, which gradually reduce in thickness towards the marginal area (Moribayashi and Maruo 1980). These thick sediments are derived mainly from the surrounding hills of the valley. The valley sediments consist of peat, clay, carbonaceous clay, sand, silt, and gravels. Thapa (1977) recognized three litho-facies within the valley sediments:-

Facies I: Fluvial sediment consisting gravels, sands, silt and clay in the northern half of the valley; *Facies II*: Lake Delta sedimentary Facies developed in the central part of the valley consisting sands and laminated clay and silts and *Facies III*: Lake deposit distributed in the southern half of the basin and consisting of unconsolidated mud beds, thin beds of fine sand and diatomaceous earth.

Yoshida and Igarashi (1984) classified the Kathmandu Valley sediment into eight stratigraphic units and also carried out radiometric dating, paleomagnetic measurements and pollen analysis of the sediments. The main compositions of eight lithostratigraphic units are given in table 1.1.

Table 1.1: Classification of Kathmandu Valley Sediment (after Yoshida, 1984)

Stratigraphic Unit	Composition	Distribution
Recent Flood Plain deposits (Holocene)	Sand, silt and clay	Along Bagmati River and its tributaries

Lower Terrace deposits (Holocene)	Micaceous sand and gravel	Along Bagmati River and its tributaries
Patan Formation (Pleistocene)	Laminated arkosic sand, silt, clay and peat layers	Mainly around Patan and Kathmandu city
Thimi Formation (Pleistocene)	Laminated arkosic sand, silt, clay and peat	North part of Kathmandu around Gokarna area
Gokarna Formation (Pleistocene)	Laminated arkosic sand, silt clay and peat	North part of Kathmandu around Gokarna area
Boregaon Terrace deposit (Pleistocene)	Rounded gravel with laminated silt and sand	Southern areas of Kathmandu valley near Pyangaon and Godavari village
Pyangaon Terrace deposit (Pleistocene)	Subrounded gravel of metasandstone and phyllite	Southern area of Kathmandu valley near Pyangaon and Godavari village
Lukundol Formation (Pleistocene)	Weakly consolidated clay, silt and sand beds with lignite layers	Along terrace, scarps near Chapagaon village, probably widely distributed in the subsurface ot the valley

Dangol (1985) reported the presence of vertebrate fossils in the lignite of the Lukundol Formation and subdivided the Lukundol Formation into Basal Conglomerate, Lignite Member, Laminated Silt Member and Upper Gravel Member.

Sah et al. (1997) classified the lithological succession of the Kathmandu Valley into Tarebhir Conglomerate, Lukundol Formation, Sunakothi Formation, Sankhu Formation, Gokarna Formation, Thimi Formation and Kalimati Clay. They also

recorded the fossil contents of an early Pleistocene diatomite section exposed along Nakhu Khola.

Sakai (2001) divided the Kathmandu basin sediments into Tarebhir, Lukundol, and Itaiti Formations in the southern part, and into Bagmati Formation, Kalimati Formation with Basal Lignite Member, and Patan Formation in the central part of the Kathmandu valley.

Sakai T. et al. (2001) reported the deltaic deposition with sedimentary architecture of delta plain, delta front, and prodelta successions in the Gokarna and Thimi Formation, distributed in the central and northern part of the valley. From the aggrading delta-plain deposits, they recognized small-amplitude lake-level fluctuations.

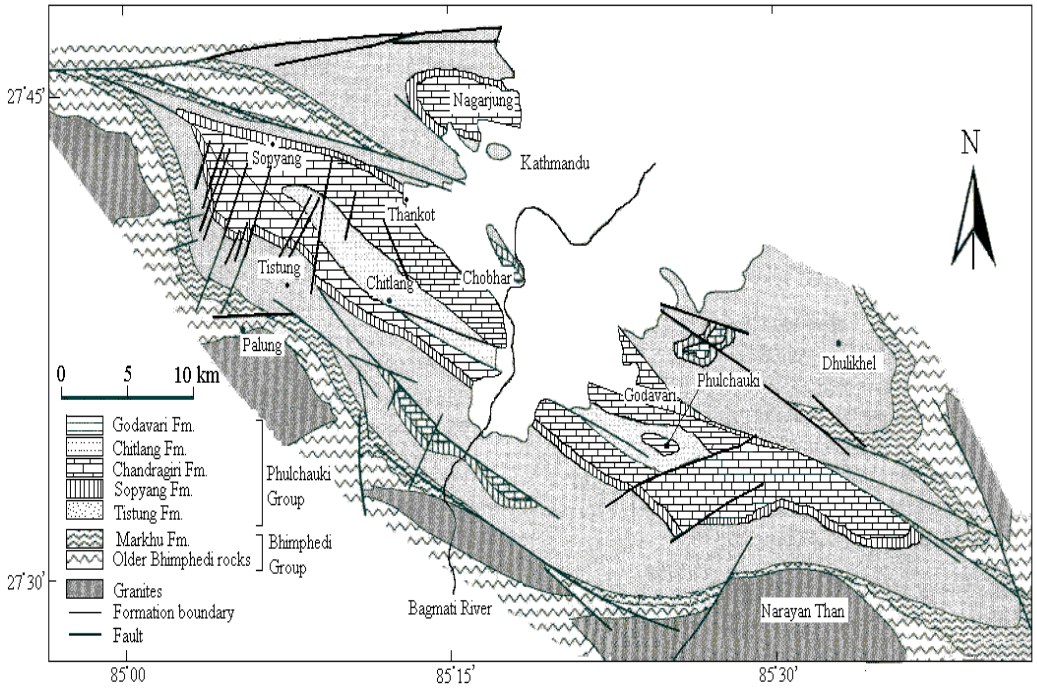

Fig.2.1 ***Simplified Geological Map of Kathmandu area (after Stöcklin 1980)***

2.3 Holocene Geology

Alluvial cover of the Bagmati River terraces are found not to be very thick as they underwent repeated depositional and erosional cycles. The thickness of Holocene sediments in the Bagmati River valley varies mostly from 0.5 to 6 m.

Bagmati River valley, between Sundarijal and Chobhar, can be divided into different depositional zones with specific local environment conditions. The identified zones have their characteristic geomorphological and sedimentological peculiarities and are demarcated by active faults.

Five environmental geological distinct zones between Sundarijal and Chovar (Gurung, J.K., 1996) are recognized as follows:

Sundarijal Gokarna Alluvial Terrace

Gokarna Alluvial Terrace

Gairigaon Alluvial Terrace

Sankhamul Fan Terrace

Sankhamul Chobhar Terrace

2.4 Seismo-tectonic of the Area

Kathmandu area is seismically very active and has experienced several devastating earthquakes in the past. Seismological records have indicated that there are several seismically active faults in the area. Fig. 2.1 shows various faults around Kathmandu area. Appendix X shows various Earthquake sources and their hypocentral distance.

CHAPTER THREE

THEORY OF ELASTICITY AND SEISMIC WAVES

3.1 The Elastic Wave Model

The basic physical model in seismology is that of a perfectly elastic medium in which the infinitesimal strains approximation of elasticity theory is adopted. If the Cartesian coordinates of a point A of the medium are given by x_i (i = 1, 2, 3), after passage of seismic wave, let A be displaced by an amount u_i ; then a neighboring particle B, initially at $x_i + dx_i$, is displaced an amount

$$U_i + \frac{\partial u_i}{\partial x_j} dx_j \text{.....(3.1)}$$

Where the convention is that a repeated suffix stands for the summation over that suffix.

A measure of the deformation is

$$d(AB)^2 = \left(\frac{\partial u_j}{\partial x_i} + \frac{\partial u_i}{\partial x_j}\right) dx_i dx_j + \frac{\partial u_i \partial u_i}{\partial x_j \partial x_k} dx_j dx_k$$

$$= 2\, e_{ij}\, dx_i\, dx_j + \text{second-order terms,}$$

Where

$$e_{ij} = \frac{1}{2}\left(\frac{\partial u_j}{\partial x_i} + \frac{\partial u_i}{\partial x_j}\right) \quad \text{..... (3.2)}$$

For infinitesimal strain, the second-order terms are neglected. Because of its symmetry the (infinitesimal) strain tensor e_{ij} has only six independent components of which e_{11}, e_{22}, e_{33} correspond to *extensions* parallel to the Cartesian axes and e_{23}, e_{31}, e_{12} measure the angular deformation or *shear strain*.

The increase in volume of a unit cube of the medium through rarefaction is $e_{11} + e_{22} + e_{33} = e_{ii}$, to first order. In the limit, as the volume becomes vanishingly small, e_{ii} is a measure of the *dilatation* θ or negative compression. On this infinitesimal strain theory, the deformation of the ground is a function only of the derivatives $\partial u_i / \partial x_j$.

Thus, using Eq. 3.2,

$$\frac{\partial u_i}{\partial x_j} = e_{ij} - w_{ij}$$

Where,

$$w_{ij} = \frac{1}{2}\left(\frac{\partial u_j}{\partial x_i} - \frac{\partial u_i}{\partial x_j}\right) \qquad \text{..... (3.3)}$$

The ground deformation is thus the resultant of strain e_{ij} and rotation w_{ij}.

Translation and deformation of an elastic body are conceived as arising from the application of two types of forces: body forces and surface tractions. The *stress* at a point A of the medium arises from the surface tractions on small plane interfaces surrounding the point. As the area of the interfaces becomes vanishingly small the ratio of the tractions to the area is called the stress at A. These pressures may be summarized by a symmetrical *stress tensor* p_{ij}. If the reference axes are selected so that the shear components p_{23}, p_{31}, p_{12} are all zero, the components p_{11}, p_{22}, p_{33} are the principal stresses at A.

For hydrostatic pressure p, the three principal stresses will each equal minus p. More generally, let P be the mean of the principal stresses, i.e.,

$$P = (1/3)p_{ii}$$

Then the applied stresses can be treated as the resultant of the mean stress P together with deviations P_{ij} from it.

In symbols,

$$P_{ij} = p\,\delta_{ij} + P_{ij} \qquad \text{..... (3.4)}$$

Where P_{ij} is the stress deviator tensor and δ_{ij} *is Kronecker delta.*

In corresponding physical representation, the strain deviator *Eij* is given by,

$$e_{ij} = \left(\frac{1}{3}\right)\theta\delta_{ij} + E_{ij} \qquad \text{..... (3.5)}$$

3.2 Stress – strain Relationship

For many seismological purposes, stress is taken to be related to strain though Hooke's relation, which is both linear and time invariant. Hooke's law is the basic law in elasticity and it states that the extension produced in an elastic body is

directly proportional to the force producing it. However, this proportionality holds well within a certain limit of deformation. This limit is called the proportionality limit. Beyond the proportionality limit, Hooke's law no longer holds. Although the material is still elastic and returns to its original shape when stress is removed, the stress-strain relationship is non-linear (Fig. 3.1). If a solid is deformed beyond a certain point, known as the elastic point, it will not recover its original shape when stress is removed. In this range a small increase in applied stress causes a disproportionately large increase in strain. The deformation is said to be plastic, if the applied stress is removed in the plastic range, the strain does not return to zero; a permanent strain has been produced. Eventually the applied stress exceeds the strength of the material and failure occurs. It is named as the ultimate strength of the material. In some rocks failure can occur abruptly within the elastic range; this is called brittle behavior.

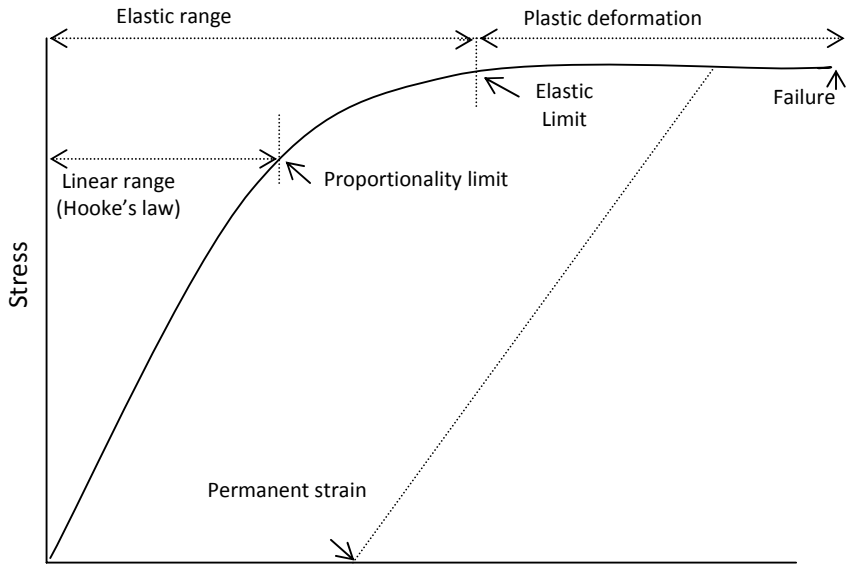

Fig. 3.1: ***The stress-strain relation for a hypothetical solid is linear (Hooke's law) until the proportionality limit, and the material deforms elastically until it reaches the elastic limit; plastic deformation produces further strain until failure occurs (Lowrie, 1997)***

Anisotropy, imperfections in elasticity, and gross geological inhomogeneities also effect the ground response predicted by the simpler theory (Wiegel, Robert

L., Earthquake engineering). An *isotropic medium* has complete elastic symmetry. Its elastic behavior is described completely by two coefficients λ and μ, where μ is the ***Rigidity Modulus*** of the medium and $\lambda = k - \frac{2}{3}\mu$; k is the ***Incompressibility*** or ***Bulk Modulus,*** defined as the ratio of hydrostatic pressure to resulting volume change. The full stress–strain relations for a perfectly elastic isotropic medium are

$$p_{ij} = \left(k - \frac{2}{3}\mu\right)\theta\delta_{ij} + 2\mu e_{ij} \qquad \text{..... (3.6)}$$

From the ratio of the transverse strain (contraction) to the longitudinal strain (extension) of an elastic cylinder, subject to uniform tension over its plane ends and free from lateral traction, a useful relation between k and μ may be derived that is called ***Poisson's ratio*** σ :

$$\sigma = \frac{3k-2\mu}{2(3k+\mu)},$$

Where $-1 < \sigma < ½$

For a fluid $\sigma = 0.5$, for granitic rocks $\sigma \approx 0.21$, and for the sedimentary column of the Earth's crust (average density about 2.4 gm/cm^3) $\sigma \approx 1/3$. The assumption $\sigma = 0.25$, called *Poisson's relation*, is sometimes used as an approximation to simplify the mathematical development.

The ratio of extensional stress to resulting extensional strain for a cylinder being pulled on both ends is defined as ***Young's Modulus*** (E). It can be shown that,

$$E = \frac{(3\lambda+2\mu)\mu}{\lambda+\nu}$$

Consider an element, with volume dV and surfaces dS, of a continuous perfectly elastic medium of density ρ. Suppose that the equilibrium state at time t is perturbed by an earthquake that changes the body force per unit mass by X_i and the stress by p_{ij}. The element will suffer acceleration, $\partial^2 u_i/\partial t^2$ approximately, so that, by Newton's law,

$$\int_v \rho\left(\frac{\partial^2 u_i}{\partial t^2}\right) dV = \int_s \nu_j P_{ji} dS + \int_v \rho X_i dV \text{.....(3.7)}$$

On the assumption of continuous and single-valued functions p_{ji} and their derivatives, Gauss's divergence theorem yields,

$$\rho\left(\frac{\partial^2 u_i}{\partial t^2}\right) = \frac{\partial p_{ji}}{\partial x_j} + \rho X_i \ldots\ldots\ldots\ldots\ldots \quad (3.8)$$

$i,j = 1,2,3$

The three partial differential equations (Eq.3.8) are called the *basic equations of elastic wave theory*. For a non-homogeneous but isotropic medium, substitution from Eq.3.6 gives,

$$\rho\frac{\partial^2 u_i}{\partial t^2} = \left(\frac{\partial}{\partial x_i}\right)\left[\left(k - \frac{2}{3\mu}\right)\theta\right] + \left(\frac{\partial}{\partial x_j}\right)\left[\mu\left(\frac{\partial u_j}{\partial x_i} + \frac{\partial u_i}{\partial x_j}\right)\right] + \rho X_i \ldots\ldots\ldots \quad (3.9)$$

It can be shown that the usual body forces, e.g., gravity, produce insignificant effects on short-period seismic waves. Therefore, omitting the X_i term and the gradients of k and μ, the Eq. 3.9 becomes,

$$\rho\frac{\partial^2 u_i}{\partial t^2} = \left[\left(k + \frac{1}{3}\mu\right)\frac{\partial\theta}{\partial x_i}\right] + \mu\nabla^2 u_i \ldots\ldots\ldots\ldots\ldots \quad (3.10)$$

Following the method used by Helmholtz in electromagnetic theory, we may analyze the time variations of the vector displacements u_i by putting,

$$u_i = \frac{\partial\varphi}{\partial x_i} + (curl\ \psi)_i$$

Where φ is a scalar and ψ is a vector potential. Then div $u = \nabla^2\varphi = \theta$

Substitution in the equation of motion Eq. 3.8 demonstrates that they are satisfied if,

$$\rho\left(\frac{\partial^2\varphi}{\partial t^2}\right) = \{k + \left(\frac{4}{3}\right)\mu\}\nabla^2\varphi \ldots\ldots\ldots\ldots (3.11)$$

And

$$\rho\left(\frac{\partial^2\psi}{\partial t^2}\right) = \mu\nabla^2\psi \ldots\ldots\ldots (3.12)$$

The expression Eq.3.11 is the wave equation for waves of dilatation with velocity

$$\alpha = \sqrt{\frac{\left[k+\left(\frac{4}{3}\right)\mu\right]}{\rho}} \text{ ..... (3.13)}$$

And Eq.3.12 is the equation for shear waves with velocity

$$\beta = \sqrt{\frac{\mu}{\rho}} \text{ ..... (3.14)}$$

In a fluid (i.e., μ = 0) there are no shear waves and in a gas, $\alpha = \sqrt{\frac{k}{\rho}}$

3.3 Body Waves

In seismology, the dilatational waves are called *P* (primary) waves and the shear waves are called *S* (secondary) waves. From a source within an elastic medium, both types of body waves will propagate outward into the medium. If the source can be approximated by a point or small sphere, the wave fronts will be spherical in a homogeneous isotropic medium; at large distances from a source of arbitrary shape the wave fronts are effectively plane, so that the *P* motion is *longitudinal* and the *S* motion is *transverse* to the direction of propagation.

A

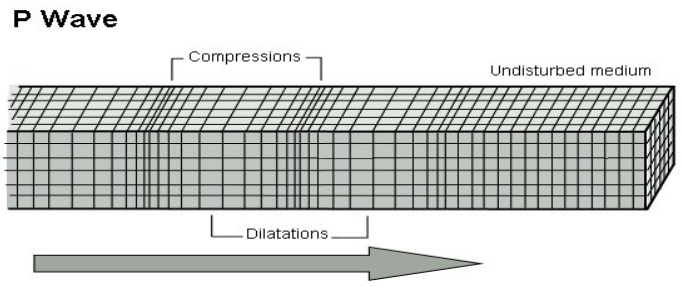

B

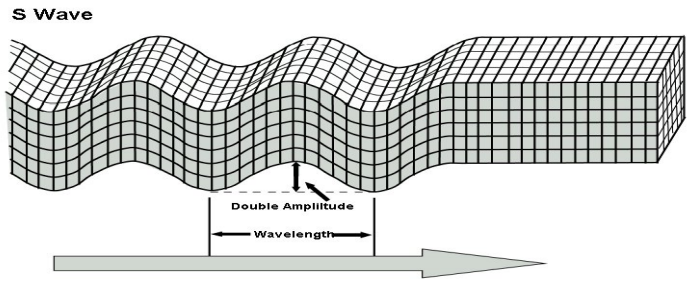

Fig. 3.2 ***Elastic deformations and ground particle motions associated with the passage of body waves: (A) P-wave, and (B) S-wave (After Bolt, 1982)***

When a body wave reaches a distance from its source in a homogenous medium, the wave front has a spherical shape, and the wave is called a *spherical wave*. Shear waves from an earthquake travel more slowly than primary waves and are recorded at an observation station at later arrivals.

3.4 Polarization of P- and S- waves

It may be further demonstrated that *S* plane waves may be plane-polarized. In the Earth, polarization is observed and relative to the Earth's surface, *S* waves that cause particles of the medium to move in a vertical plane containing the direction of propagation are denoted by *SV*; horizontally polarized waves are called *SH* waves.

When an elastic body wave encounters an interface or boundary that separates rock of different elastic properties it will, like sound and electromagnetic waves, undergo reflection and refraction. There is the special complication in the elastic wave case that conversion between mode types occurs: either an incident *P* or *SV* wave can yield, in general, reflected *P* and *SV* waves and refracted *P* and *SV* waves; an incident *SH* wave yields only reflected and refracted *SH* waves.

P-wave velocity of different materials is shown in Table 3.1.

Table 3.1: P-wave velocities through some materials (after Reynolds, 1997)

Material	Velocity (m/s)	Material	Velocity (m/s)
Air	330	Limestone (hard)	2800-7000
Water	1450-1530	Dolomites	2500-6500
Petroleum	1300-1400	Anhydrite	3500-7500
Loess	300-600	Rock Salt	4000-5500
Soil	100-150	Gypsum	3000-3500
Snow	350-3000	Shales	2000-4100
Solid Glacier ice	3000-4000	Granites	4600-6200

Sand (loose)	200-2000	Basalts	5500-6500
Sand (dry, loose)	200-1000	Gabbro	6400-7000
Sand (water sat., loose)	1500-2000	Peridotite	7800-8400
Glacial moraine	1500-2700	Serpentinite	5500-6500
Sand and gravel (near surface)	400-2300	gneiss	3500-7600
Sand and gravel (at 2 km depth)	3000-3500	Marbles	3780-7000
Clay	1000-2500	Sulphide ores	3950-6700
Estuarine mud/ clay	300-1800	Pulverized fuel ash	600-1000
Floodplain alluvium	1800-2200	Made ground (rubble etc.)	160-600
Permafrost (Quaternary sediments)	1500-4900	Landfill refuse	400-750
Sandstone	1400-4500	Clay landfill cap (Compacted)	355-380
Limestone (soft)	1700-4200	Disturbed soil	180-335
Concrete	3000-3500		

In solids comparison between α and β shows that

$$\alpha^2 - \frac{4}{3}\beta^2 = \frac{k}{3} \text{ ..... (3.15)}$$

The velocity ratio of seismic body waves is a very useful parameter for the determination of Poisson's ratio. The relation is

$$\left(\frac{\alpha}{\beta}\right)^2 = \frac{1-\sigma}{\frac{1}{2}-\sigma} \text{ ..... (3.16)}$$

Typical values of Poisson's ratio are given in Table 3.2. The Poisson's ratio can be calculated by using P-waves and density of the materials as,

$$\sigma = \alpha^2 \rho \frac{(1-2\sigma)(1+\sigma)}{1-\sigma} \ldots\ldots\ldots\ldots \quad (3.17)$$

Table 3.2: Typical values of Poisson's ratio (Arora, 2000)

S.No.	Types of soil	Poisson's ratio
1	Saturated clay	0.4-0.5
2	Unsaturated clay	0.1-0.3
3	Silt	0.3-0.35
4	Loose sand	0.3-0.5
5	Dense sand	0.2-0.3

3.5 Physical Factors that affect P- & S- wave Velocity

For given sediment, the velocity depends mainly on porosity, pressure and water saturation. Different sediment types are characterized by different velocity values and velocity dependencies of controlling parameters. These are controlled by differences in the mineralogical composition, grain size distribution and grain shape etc.

In consolidated sediments P-wave velocity depends on the porosity and on the material filling the pores. The velocity generally increases as the porosity decreases. The relationship given by Wyllie et al. (1958) is

$$1/\alpha = \emptyset/\alpha_f + (1-\emptyset)/\alpha_m \ldots\ldots\ldots\ldots\ldots\ldots \quad (3.18)$$

Where, α and $\emptyset$ are velocity of P-wave and porosity respectively, while α_f and α_m are acoustic velocities in the pore fluid and the rock matrix respectively. Typical values for the α_f and α_m are 1500 m/s, and 2800 m/s respectively.

P-wave velocity is higher for denser rock. An empirical relationship given by Gardner et al. (1974) shows the increase in P-wave velocity with density,

$$\rho = 0.31\ V^{1/4} \text{.....} \quad (3.19)$$

Where ρ is the density in g/cm^3 and V is P-wave velocity in m/s.

The seismic wave velocities in sedimentary rocks in particular increase both with depth of burial and age. The relationship is given by Faust (1951),

$$V = 1.47\ (ZT)^{1/6} \text{ Km/s} \text{ .....} \quad (3.20)$$

For Shale and sands where Z is the depth (Km) and T is the geological age in millions of years.

There exists significant correlation between velocity and porosity for unconsolidated sediments (Schon, 1983). Velocity values in unconsolidated sediments are distinctly lower than in consolidated sediments. The longitudinal wave velocity has particularly a clear difference in velocity for the dry (about 200-500 m/s) and water saturated (about 1600-2000 m/s) sediment (Schon, 1983). The differences between the velocities in dry and water saturated state increase with increasing porosity and decreases with increasing pressure (Nur and Simmons, 1969). The influence generally is much stronger for P-waves due to the distinct difference of the compressibility of fluids and gases than for S-waves where only the change of the density and boundary effects play a role. There is also a substantial amount of velocity change under the influence of lower pressure range. At lower pressure range, there is a marked increase of velocity with depth. At higher pressures i.e. at great depths, the compaction of the aggregate is nearly complete and the further velocity increase is due to the change of the elastic properties of the minerals and clasts. Morgan (1969) has derived a set of linear and quadratic relations between velocity and porosity velocity and grain size and velocity and void ratios.

With increasing amount of clay the velocity generally decreases in unconsolidated sediments. This is the result of the low stiffness of the clay-water aggregates in the sediments. The transverse wave velocity also decreases with clay content. Generally the effects of porosity and amount of clay on shear wave velocity V_s are larger than on the compressional velocity V_p (Han, Nur and Morgan, 1986). Increasing porosity and clay content results decrease in longitudinal wave velocity, whereas an increasing carbonate content leads to a

stabilization of the sediment skeleton and, therefore, to increasing stiffness, and thus to an increasing shear wave velocity.

Unconsolidated sediments can be distinguished into: noncohesive e.g. sand, gravel and cohesive e.g. clay. The differences in the features of these two groups are based on various physical conditions at the contacts of the particles. In the first group the conditions are controlled by friction effects and in the second group physicochemical phenomenon are dominant. The different grain shapes have different contact conditions among the grains. In dry state P-wave velocity has "frame determined" behavior. In saturated state, P-wave has "pore determined" behavior. But in both states for the S-wave it has generally" frame determined" behaviors.

As a result of technological advance, more transverse wave velocity data have become available in exploration, well logging and other engineering applications. Han, Nur and Morgan (1986) noted that "the combined use of the velocity and velocity ratio provide a useful tool for reliable discrimination of lithology especially for rocks". The classic paper by Pickett (1963) recommended the V_p/V_s ratio as a lithology indicator. The combined effect of clay and porosity on V_p/V_s has been investigated by Castanga et al. (1985), Tosaja and Nur (1982) and Hornby and Murphy (1987). The ratio V_p/V_s decreases with increasing transverse wave velocity and increases with decreasing transverse velocity. A sample with high porosity and clay content tends to have a higher V_p/V_s ratio. Increasing transverse velocity reflects an increase of compaction and decrease of porosity. This causes a corresponding decrease of V_p/V_s with increasing depth.

3.6 Static and Dynamic Moduli

A point noteworthy to mention is that the modulus of elasticity determined by static (application of static loads) and dynamic methods (application of dynamic loads) are not the same. The moduli of elasticity determined from dynamic methods are larger than those determined from static methods. Masuda (1960) reported that the ratios of these moduli of elasticity were about four to five. The mean values for the ratio E_{dyn}/E_{stat} for unconsolidated sediments are as great as

5 for cohesion less and 20 for cohesive soils (Schon, 1998). Table 3.3 gives an overview of the mean ranges of the two young's moduli.

Table 3.3: Static and dynamic Young's modulus for unconsolidated rocks (after Schon, 1983)

Sediment Type	Description	E_{stat} (MPa)	E_{dyn} (MPa)
Cohesionless	Gravel	100-200	300-800
	Sand lose	40-100	150-300
	Sand dense	80-200	200-500
Cohesive	Clay hard	10-50	50-500
	Clay soft	3-6	30-80
	Boulder clay	6-35	100-500

Due to the large variations in the ratio of the dynamically and statically determined modulus, a strong correlation cannot be determined (Schon, 1998). However one physical basis for a correlation is the fact that both moduli depend on the porosity and show remarkably similar pressure dependence. Gorjainov and Ljachowickis (1997) have given an equation relating static and dynamic young's modulus from shallow seismic measurements and soil mechanic tests for a depth of up to 10m. The equation is

$$E_{stat} = E_{dyn} + b \quad \text{..... (3.21)}$$

Some mean values for the co-efficient *a* and *b* are given in Table 3.4.

Table 3.4: Mean values for the co-efficient of the regression equation (after Gorjainov and Ljachowickis; 1979)

Soil type	*a*	*b* in MPa
Sand wet	0.085	3

Clay	0.033	6.5
Soil, wet, sandy	0.061	2.85

3.7 Surface Waves

Waves that do not penetrate deep into sub-surface media are known as surface waves, of which there are two types, *Rayleigh* and *Love* waves. Rayleigh waves travel along the free surface of the Earth in the same way that a wave rolls across a lake or an ocean, moving the ground up and down or side to side in the same direction that the wave is moving with amplitudes that decrease with depth. The particle motion is actually a retrograde ellipse in a vertical plane with respect to the direction of propagation (Fig.3.3). The major axis is vertical and minor axis is in the direction of wave propagation. In 1885 Lord Rayleigh described that the part in the wave front of the Rayleigh wave are polarized to vibrate in the vertical plane. The resulting particle motion can be regarded as a combination of the *P*-and *SV*- vibrations.

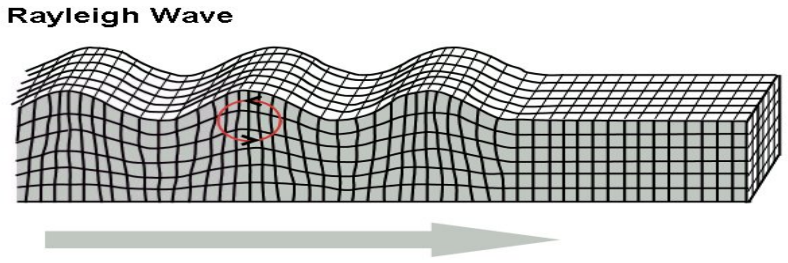

Fig. 3.3: ***Elastic deformations and ground particle motions associated with passage of Rayleigh wave (After Bolt, 1982)***

In 1911 A.E.H. Love showed that if a horizontal layer lies between the free surface and semi-infinite half space (Fig. 3.4) horizontally polarized shear waves (*SH*-waves) within the layer that are reflected at supercritical angles from the top and bottom of the layer can interfere constructively to give a surface-wave with horizontal particle motions. These waves are called Love waves. The

velocity (β_1) of shear waves in the near-surface layer must be lower than in the underlying half-space (β_2) for the generation of love waves. The velocity of the Love waves lies between the two extreme values: $\beta_1 < V_L < \beta_2$. Of the surface waves, love waves travel at approximately the same speed as shear waves as they are polarized shear waves, but Rayleigh waves travel slightly slower at about 0.92 V_s (for Poisson's ratio 0.25).

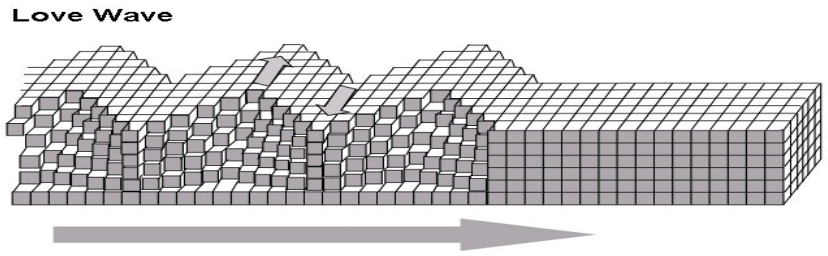

Fig. 3.4: ***Love wave propagation with particle motion horizontal and perpendicular to the propagation of wave (Bolt, 1982)***

The speed of Love waves with very short wavelengths is close to slower velocity β_1 of the upper layer, while Long wavelengths travel at a speed close to the faster velocity β_2 of the lower medium. This dependence of velocity on wavelength is termed dispersion. Love waves are always dispersive because they can only propagate in a velocity-layered medium.

3.8 Dynamic Properties of Soil

The response of soils to cyclic loading is controlled mostly by the mechanical properties of the soil. There are several types of geotechnical engineering problems associated with dynamic loading, some examples include: wave propagation, machine vibrations, seismic loading, liquefaction and cyclic transient loading, etc. The mechanical properties associated with dynamic loading are shear wave velocity (Vs), elastic modulus (E), shear modulus (G), damping ratio (D), and Poisson's ratio (ν). The customary name for this type of properties is "dynamic soil properties," even though they are also used in many non-dynamic type problems, the engineering problems governed by wave

propagation effects induce low levels of strain in the soil mass. On the others hand, when soils are subjected to dynamic loading that may cause a stability problem then, large strains are induced.

Dynamic soil properties also require an active source of energy to excite the soil mass and/or induce a measurable wave. Geophysical tests propagate seismic waves through soil at a very low strain level (less than 10^{-3} percent), making practically impossible the measurement of strain. This low level of strain allows the use of elastic theory to associate measurements with mechanical properties and for the most part the response linear. At large strains ($\sim 10^{-1}$ to 5 percent) the dynamic behavior of soils remains non-linear and will begin experiencing permanent deformation (plastic) and eventually reach an unstable condition. For intermediate and large strains geophysical properties are not applicable anymore and specialized laboratory soil tests such as cyclic tri-axial shear tests are used. In summary, dynamic soil properties are strain-dependent and one of the challenges is having compatibility in the results of the different methods when the strain level overlaps.

Most seismic geophysical methods or tests induce shear strains lower than 10^{-4} % and the shear wave velocity (Vs) can be used to computed the G_{max} using the expression $G_{max} = \rho.V_s^2$, where ρ is the mass density of the soil. The measured shear wave velocity is generally considered the most reliable means to obtain the G_{max} for a soil deposit. These methods involve the creation of a transient and/or steady – state stress waves (source) and the interpretation of the arrival time and spectral response at one or more locations (receivers). The generation of the impulse wave by the source can vary from a sledge hammer blow at ground surface, to a buried explosive charge or to an active varied frequency source vibrator.

CHAPTER FOUR

MEASUREMENT OF SEISMIC VELOCITIES

4.1 Vertical Seismic Profiling

Vertical Seismic Profiling (VSP) is an effective seismic surveying which needs boreholes, one or more than one. Seismic detectors are located at known levels within a borehole and shots fire at the surface and vice-versa. Two types of borehole seismic loggings are used (i) Up-hole seismic logging and (ii) Down-hole seismic logging. During this study seismic down the hole logging has been used for shallow sub-surface analysis.

4.2 Down the Hole Compressional and Shear wave Test

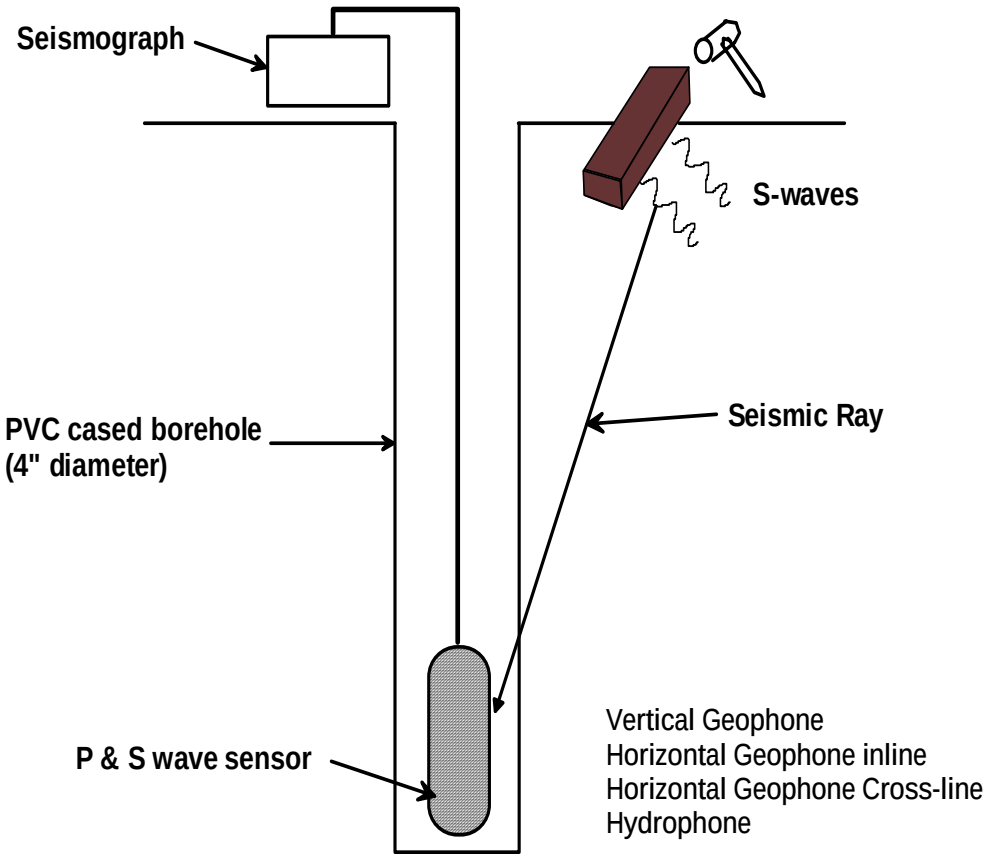

Fig. 4.1: Schematic diagram for Down the hole seismic survey

The basic layout of a down the hole compressional and shear wave test is shown schematically in figure 4.1.

4.2.1 Background

A significant advancement in the study of Down the Hole Seismic testing was made by Dr. Kenneth in introduction of the "Interval Velocity" concept. The key to reliable interpretation of the downhole test was the distinction between and appropriate interpretation of true and pseudo interval approaches to velocity determination.

4.2.2 Direct Arrival Approach

In the direct arrival approach, a single transduction is lowered in a borehole and velocities of the soil layers encountered are determined from the slope of a best fit curve through the data points on a travel time plot.

4.2.3 True Interval Method

In the true interval method, the difference in time between the arrivals of a seismic wave at each of two geophones situated a fixed distance apart is used as the travel time over the distance between geophones.

4.2.4 Pseudo-Interval Method

In the pseudo-interval method, the time difference between wave arrivals at a single geophone at two successive known depths is used as a travel time for the difference in depth. The Pseudo-Interval method was the next best approach and if carefully executed provided good velocity profiles.

Another advance in insitu test resulted from the coupling the downhole test with static cone penetrometer test. This combined test was first reported by Robertson et al. (1985) and is called the seismic cone penetrometer test (SCPT). The shear wave velocities obtained this way can then be used to compute shear modulus which in turn can be used in conjunction with the cone bearing and friction ratio data from the cone penetration test.

4.3 Equipment

The instruments used were the seismic source- sledge hammer, metal base plate, wooden block, a probe consisting of vertical and horizontal geophones, seismic cable and seismograph. The seismograph used in the survey is the McSEIS –170f, a handy size (with dimensions of 390mm (L) × 335mm (H) × 370mm (B), and weight approximately about 18 kg), (shown in plate Fig.4.2) 24-channels seismograph of digital stacking type housing in the IFP (Instantaneous Floating Point) Amplifier, manufactured by OYO Corporation, Japan.. The adoption of IFP Amplifier has made it feasible to obtain the data of high quality with the attainment of wide dynamic range.

Fig. 4.2: ***Seismograph used in data acquisition***

The instrument has a high speed of A/D conversion of the level of 50μsec (whereas "25μsec" in case of 12 channels put in function) with 12 – bit (± 5V FS) and dynamic range equivalent to 20 – bit. The sampling rate can also be adjusted to 100, 200, 500, 1000, 2000, or 5000 μsec. The stacking capability of the instrument helps in enhancing the pertinent significance signals with removing non-coherent noise. Stacking can be of preview or auto type. The instrument has

input impedance of 20 kΩ/ 0.005 μF. The input conversion noise level is 0.4V rms. The frequency band is 5 ~ 4000Hz, with notch at 50 Hz (typical), low-cut at 5, 30 Hz, and high-cut at 62, 250, 1000, and 4000 Hz.

Built in software functions, such as high-cut and low-cut filter, will linearly normalize to adjust the maximum amplitudes of all the channels represented within a fixed scope. Again, the system is provided with the gain facilities up to 34 dB. In the instrument fixed gain control can be adjusted beside the automatic gain control (AGC). This facilitates the ease of picking-out the first arrival waveform with sharp perception in the refraction survey. The in-phase signal elimination ratio is 100 dB. These features incorporated in the instrument makes the system ideal for the shallow reflection and refraction survey, where high resolution is required.

Real-time display of the signals is made available on 5.5 – inch CRT screen, or can be printed to hard copy with incorporated thermal type plotter. The data can be transferred to the plug-in computer, or stored on the floppy disks for later processing. The working power supply ranges within 10.8 ~ 13.2 V (3A during measurement and 5A during printing), and is provided by the rechargeable battery. The system can work in temperatures between 0 ~ 40 $^{\circ}$C.

4.3.1 Sensing Probe and Sensing Cable

In a prepared borehole with PVC casing up to a depth of 30 m from the surface, the sensing probe was suspending with a seismic cable. Sensing probe consists of 4 sensors: vertical geophone, horizontal inline geophone, horizontal cross-line geophone and hydrophone. These units are gimbaled in a cylindrical housing. The probe was kept in the borehole and the measurement was carried out at an interval of 1 m. The probe was manufactured by Geo Space, Houston, USA. The seismic cable connects the two terminals of the geophone with the seismograph. A rubber tube was suspended and attached to the sensing probe. This rubber tube when pumped expands and exerts pressure on the sensing probe such that the probe remains firmly attached to the PVC casing.

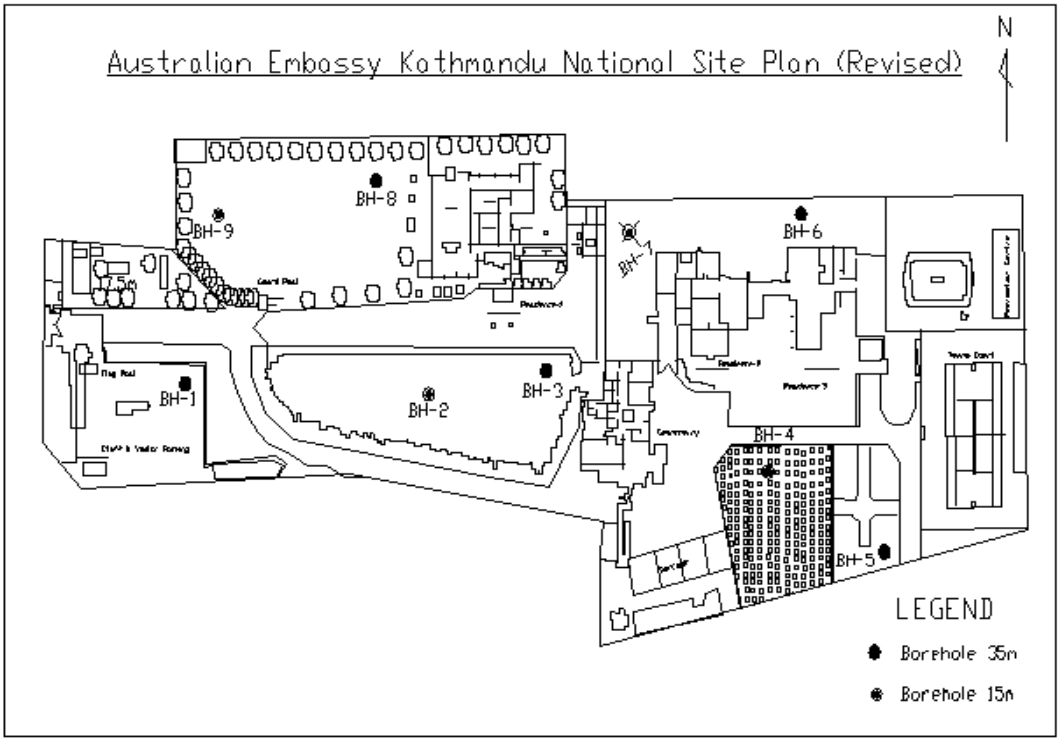

Fig. 4.3: ***Location of Boreholes inside Australian Embassy Chancery***

4.4 Methodology

Down the hole compressional and shear wave test were carried out in three boreholes: Borehole No.3, Borehole No. 5 and Borehole No.8. The maximum depth of the test was 29 m. Shear waves were generated by hitting the opposite sides of a log in horizontal direction to create predominantly SH polarized wave. The log was 2.5 m long and was kept at 3 m away from the drill hole.The compressional wave was generated by hitting on metallic plate in vertical direction. Two opposite strokes were made in order to produce shear waves of opposite polarity. Measurements were carried out in PVC cased Boreholes. These waves propagate down into the ground where they were detected by the stationary probe sensor. The single sensing probe first detected the signal at the bottom of the borehole. Then the probe was moved by 1 m towards up. The signals were similarly generated as the previous one and they were recorded. This procedure was repeated at the intervals of 1 m until the whole borehole was logged.

Fig. 4.4: ***Field layout for P-wave and S-wave data acquisition.***

The data were recorded in floppy disk. Code FIRSTPIX, developed and marketed by INTERPEX Limited from USA, was used for visualization and for picking of first arrival of shear waves and compressional waves. The option Combine Opposite Polarity was used for visualization and first arrival pick up for shear waves. By combining the opposite polarity records maximum amplitudes are obtained for the shear waves and minimum for the compressional wave. Example of the field records is presented in Appendix-I and Appendix –II.

Corrections for the vertical travel time picked up from seismogram were made by using the following formula:

$$T' = T \cos\theta \quad \ldots\ldots\ldots\ldots\ldots\ldots\ldots\ldots\ldots\ldots (4.1)$$

Where, $\theta = \tan^{-1}(L/D)$

L- Distance between drill hole and seismic source, m

D- Depth to the probe from the surface, m

T- Original travel time, ms

T'- adjusted travel time, ms

The details of the calculations for Borehole No.3, Borehole No. 5 and Borehole No.8 are presented in Appendix – IV, Appendix – V and Appendix – VI.

Travel times vs. depths were plotted for both compressional waves and shear waves first arrival pick up. Each linear segment in the graph indicates one velocity zone. The details of the compressional and shear wave velocities are presented in Appendix – II and Appendix - III.

CHAPTER FIVE

DATA ANALYSIS AND INTERPRETATION

5.1 P-wave and S-wave Velocity and Dynamic Parameters

Shear wave velocity and compressional wave velocity measurement are useful to characterize soil mechanical properties. The measurements are carried out under dynamic condition so they are called dynamic properties. These properties are elastic modulus E_{dyn}, shear modulus G_{dyn} and Poisson's ratio σ_{dyn}. These parameters are measured during the soil vibration by artificially created source and they characterize the soil dynamic condition. Determination of the E, G and σ is also possible by borehole methods in static condition. Researchers have found that there are differences in the soil dynamic and static properties calculated for the same site. Static properties calculated from borehole observation cannot characterize the 3D nature of the subsurface. Soil dynamic properties measured by seismic method represents the insitu information of the volume in subsurface. Soil dynamic properties calculated from the compressional wave velocities, shear wave velocities and density information for Borehole No. 3, Borehole No. 5 and Borehole No.8 indicate that the dynamic Young's Modulus (E_{dyn}) ranges between 91 to 672 MPa, where most of the values are closer to 400 MPa. The dynamic shear modulus (G_{dyn}) ranges between 38 MPa to 238 MPa. Most of the values are around 150 or less than 150. The Poisson's ratio lies between 0.43 to 0.49. Low value of the Poisson's ratio is obtained for unsaturated material close to surface. High value of Poisson's ratio indicates the liquid state of the subsurface formation. All these parameters are presented in Table 5.1, Table 5.2 and Table 5.3 respectively.

5.2 S-wave Velocity and Ground Motion

The fluvio-lacustrine sediments in Kathmandu valley consists of stratified and inter-fingering deposits of sand, silts, clays, and gravels with some carbonaceous

mud/clay and coal seams. The Valley as a whole consists of unconsolidated sediments with thickness greater than 500 m near Baneshwor in the central part. In such a case, the layer deposited on the surface is markedly softer than the underlying layer. The hard lower ground where the shear wave velocity exceeds 500 m/s is generally considered as engineering bedrock, which exists at most 100 m below the surface. This engineering bedrock is generally called the seismic basement or base ground. The layer deposited on the top of this base ground is called surface layer.

5.3 Earthquake Motion in Alluvial Ground

5.3.1 Frequency Characteristics of Earthquake Motion

5.3.1.1 Predominant Period

It is a feature of fluvial ground that soil types of fairly different mechanical properties are found in layers. At the time of an earthquake, the chief wave motions transmitted near the surface are the surface waves and transverse (shear) waves. Since in alluvial areas, the velocity of seismic waves is usually slower in the surface portion than in the deeper levels. Transverse waves will travel roughly orthogonal to the ground surface in the surface portion of the ground and a multi reflection phenomenon occurs in the subsurface layer. As a result the ground will vibrate greatly, with the appearance of dominant vibrations of certain specific periods. These periods are called the predominant period of the ground, and are determined by the structure of the surface layer.

When the surface layer is comprised of a single layer of uniform character, the predominant period of the ground is given by the following formula,

$$T = \frac{4H}{V_s} \qquad \text{..... (5.1)}$$

Where T denotes the predominant period of the ground, H the thickness of the surface layer, and V_s the velocity of the shear wave in surface layer.

In actual ground the surface layer seldom consists of a single layer; rather a number of strata of gravel, sand, silt, clay etc. have been deposited to form a

surface layer. When there is not much difference between the properties of the various layers, the longest predominant period may be determined by using the converted velocity, *Vs*, obtained by the following relation.

$$\frac{H}{V_S} = \Sigma \frac{Hi}{V_{Si}} \qquad \text{..... (5.2)}$$

Where,

H = overall thickness of the surface layer

Hi = Thickness of each constituent layer

V_{si} = Shear wave propagation velocity within that layer

The predominant periods of vibration may be different for different magnitude earthquakes. The period is longer for large-scale earthquakes than for small local earthquakes. In these valley fill sediments, impedance is small in comparison to that in rock; moreover, since there are predominant periods, there is a possibility of particularly large vibration occurring at the time of an Earthquake. Maximum values of acceleration, velocity, and displacement are important characteristic values of earthquake motion, and it is necessary to know to what extent these are amplified by the existence of the surface layer.

The displacements on alluvial soil are many times greater than the displacement on hard rock. When the seismic wave emerges from hard rock into unconsolidated sediments, there is heavy shaking of these sediments. Relatively rapid falling off of intensity occurs as the disturbance proceeds further in the soft soil, but the intensity increases as the seismic wave is reflected from rock into unconsolidated sediments.

5.3.1.2 Surface Layer Magnification of Earthquake Motion

In these unconsolidated sediments, vibrations are amplified due to multi reflection phenomenon. K. Kanai (1962) has given the following relation by combining the results of actual measurements with theoretical calculations to express the degree of amplification quantitatively,

$$G(T) = 1 + \frac{1}{\sqrt{\left[\frac{1+k}{1-k}\left\{1-\left(\frac{T}{T_G}\right)^2\right\}\right]^2 + \left(\frac{0.3}{\sqrt{T_G}\, x\, \frac{T}{T_G}}\right)^2}} \quad \text{..... (5.3)}$$

Provided that $k = \frac{\rho_1 V_{S1}}{\rho_2 V_{S2}}$

Where,

$G(T)$ = ratio of amplification;

T= Period of component vibration of seismic wave;

T_G= predominant period of surface layer;

ρ_1= density of surface layer; ρ_2=density of base layer

V_{S1}=Velocity of seismic shear wave in surface layer; and

V_{S2}= velocity of shear wave in base ground.

The ground amplifications for combinations of different predominant ground periods & time periods of incoming component waves calculated from above equation is given in Table 5.4.

Considering the engineering bedrock at shear wave velocity of 500 m/sec and density 2.2 gm/cm^3 at a depth of 30 m and taking the average weighted shear wave velocity of surface layer (0-30 m) to be 263 m/s and weighted average density to be 1.935 gm/cm^3, the value of 'k' used in the equation (5.3) is 0.46. The predominant period of the ground vibration observed in the borehole data is 0.5093 second and 0.4635 second in borehole 3 and borehole 8 respectively. If the incoming earthquake wave have the same period T with that of the period of the surface layer $T(G)$ maximum amplification will occur.

In the area of **Borehole No. 3** predominant period of vibration for the surface layer is 0.5 second. If the incoming earthquake wave is of this period then the wave will be amplified by factor of 3.4. In the area of **Borehole No.5** and **Borehole No.8** it will be amplified at least by a factor of 3.1.

Table 5.1: Calculation of the dynamic parameters and predominant period of the ground in Borehole No. 3

Depth m	Thick-ness H, m	V_p m/s	V_s m/s	V_p/V_s	Density g/cm3	Poisson Ratio	E_{dyn} Mpa	G_{dyn} Mpa	H/V_s s	T s
0--1	1	246	152	1.61	1.65	0.191	90.822	38.121	0.0065	0.0263
1--7	6	1355	152	8.91	1.74	0.493	120.09	40.201	0.0394	0.1578
7--22	15	1355	270	5.018	1.96	0.479	422.74	142.88	0.0555	0.2222
22--30	8	1509	311	4.852	2	0.477	571.74	193.44	0.0257	0.1028
							Predominant period (sec)			0.5093
							Predominant Frequency (Hz)			1.9633

Table 5.2: Calculation of the dynamic parameters and predominant period of the ground in Borehole No. 5

Depth m	Thickness H, m	V_p m/s	V_s m/s	V_p/V_s	Density g/cm3	Poisson Ratio	E_{dyn} Mpa	G_{dyn} Mpa	H/V_s s	T s
0--3	3	305	174	1.7528	1.7	0.2587	129.574	51.469	0.0172	0.0689
3--6	3	770	234	3.2906	1.85	0.4491	293.589	101.299	0.0128	0.0512
6--11	5	770	258	2.9845	2	0.4367	382.548	133.128	0.0193	0.0775
11--12	1	1292	258	5.0077	2	0.4792	393.855	133.128	0.0038	0.0155
12--14	2	1292	339	3.8112	2	0.463	672.533	229.842	0.0059	0.0236
14--20	6	1292	203	6.3645	2	0.4873	245.168	82.418	0.0295	0.1182
							Predominant period (sec)			0.3551
							Predominant Frequency (Hz)			2.81614

Table 5.3: Calculation of the dynamic parameters and predominant period of the ground in Borehole No. 8

Depth m	Thickness H, m	V_p m/s	V_s m/s	V_p/V_s	Density g/cm3	Poisson Ratio	E_{dyn} Mpa	G_{dyn} Mpa	H/V_s s	T s
0--4	4	403	220	1.8318	1.9	0.2877	236.84	91.96	0.0181	0.0727
4--5	1	572	220	2.6	1.9	0.4131	259.91	91.96	0.0045	0.0181
5--9	4	572	168	3.4047	1.86	0.4528	152.53	52.49	0.0238	0.0952
9--12	8	572	278	2.0575	1.97	0.3453	409.66	152.24	0.0287	0.1151
12--17	4	1350	278	4.8561	1.96	0.4778	447.72	151.47	0.0143	0.0575
17--30	9	1350	344	3.9244	2.01	0.4652	697.05	237.85	0.0261	0.1046
							Predominant period (sec)			0.4634
							Predominant Frequency (Hz)			2.1576

Table 5.4: Values of G(T) calculated from equation- 4 for k=0.46

T	T(G)																			
	0.1	0.2	0.3	0.4	0.5	0.6	0.7	0.8	0.9	1	1.1	1.2	1.3	1.4	1.5	1.6	1.7	1.8	1.9	2
0.1	2.05	1.4	1.3	1.3	1.3	1.3	1.3	1.3	1.3	1.25	1.2	1.2	1.2	1.2	1.2	1.2	1.2	1.2	1.2	1.2
0.2	1.12	2.5	1.6	1.4	1.4	1.4	1.4	1.3	1.3	1.33	1.3	1.3	1.3	1.3	1.3	1.3	1.3	1.3	1.3	1.3
0.3	1.05	1.3	2.8	1.7	1.5	1.5	1.4	1.4	1.4	1.38	1.4	1.4	1.4	1.4	1.3	1.3	1.3	1.3	1.3	1.3
0.4	1.02	1.1	1.5	3.1	1.9	1.6	1.5	1.5	1.4	1.42	1.4	1.4	1.4	1.4	1.4	1.4	1.4	1.4	1.4	1.4
0.5	1.02	1.1	1.2	1.6	3.4	2.1	1.7	1.6	1.5	1.47	1.4	1.4	1.4	1.4	1.4	1.4	1.4	1.4	1.4	1.4
0.6	1.01	1	1.1	1.3	1.8	3.6	2.2	1.8	1.6	1.56	1.5	1.5	1.5	1.4	1.4	1.4	1.4	1.4	1.4	1.4
0.7	1.01	1	1.1	1.2	1.4	2	3.8	2.4	1.9	1.69	1.6	1.5	1.5	1.5	1.5	1.4	1.4	1.4	1.4	1.4
0.8	1.01	1	1.1	1.1	1.2	1.5	2.1	4	2.5	1.96	1.8	1.6	1.6	1.5	1.5	1.5	1.5	1.4	1.4	1.4
0.9	1	1	1	1.1	1.2	1.3	1.6	2.3	4.2	2.63	2	1.8	1.7	1.6	1.6	1.5	1.5	1.5	1.5	1.5
1	1	1	1	1.1	1.1	1.2	1.4	1.6	2.4	4.33	2.8	2.1	1.9	1.7	1.6	1.6	1.6	1.5	1.5	1.5
1.1	1	1	1	1.1	1.1	1.2	1.3	1.4	1.7	2.59	4.5	2.9	2.2	1.9	1.8	1.7	1.6	1.6	1.5	1.5
1.2	1	1	1	1	1.1	1.1	1.2	1.3	1.5	1.82	2.7	4.7	3	2.3	2	1.8	1.7	1.6	1.6	1.6
1.3	1	1	1	1	1.1	1.1	1.2	1.2	1.3	1.53	1.9	2.9	4.8	3.2	2.4	2	1.9	1.8	1.7	1.6
1.4	1	1	1	1	1.1	1.1	1.1	1.2	1.3	1.38	1.6	2	3	4.9	3.3	2.5	2.1	1.9	1.8	1.7
1.5	1	1	1	1	1	1.1	1.1	1.1	1.2	1.3	1.4	1.7	2.1	3.2	5.1	3.4	2.5	2.2	1.9	1.8
1.6	1	1	1	1	1	1.1	1.1	1.1	1.2	1.24	1.3	1.5	1.7	2.2	3.3	5.2	3.5	2.6	2.2	2
1.7	1	1	1	1	1	1.1	1.1	1.1	1.1	1.2	1.3	1.4	1.5	1.8	2.3	3.4	5.3	3.7	2.7	2.3
1.8	1	1	1	1	1	1	1.1	1.1	1.1	1.17	1.2	1.3	1.4	1.6	1.8	2.3	3.5	5.5	3.8	2.8
1.9	1	1	1	1	1	1	1.1	1.1	1.1	1.14	1.2	1.2	1.3	1.4	1.6	1.9	2.4	3.7	5.6	3.9
2	1	1	1	1	1	1	1.1	1.1	1.1	1.12	1.2	1.2	1.3	1.4	1.5	1.7	1.9	2.5	3.8	5.7

5.4 Correction of N-Values

There are a number of factors involved in the SPT, which can affect the blow count, mainly related to poor testing practice (Bowles, 1968). The standard penetration number is corrected for dilatancy effect and overburden effect.

5.4.1 Dilatancy Correction

If the soil consists of very fine or silty sand below the water table, a correction is made when the measured *N* value is greater than 15, because excess pore-water pressure set up during driving cannot dissipate. The pore pressure affects the resistance of the soil and hence the penetration number (*N*). Terzaghi and Peck (1967) recommend the following correction in the case of silty fine sands when the observed value of *N* exceeds 15.

$$N_C = 15+0.5\ (N_R - 15) \quad \ldots\ldots\ldots\ldots\ldots\ldots\ldots\ldots\ldots\ldots \quad (5.4)$$

Where,

N_R is the recorded value and N_C is the corrected value.

If $N_R \leq 15$, $N_C = N_R$

5.4.2 Overburden Pressure Correction

In granular soils, the overburden pressure affects the penetration resistance. If the two soils having the same relative density but different confining pressures are tested, the one with a higher confining pressure gives a higher penetration number. As the confining pressure in cohesion-less soils increases with the depths, the penetration number for soils at shallow depths is underestimated and that at greater depths is overestimated. For uniformity, the N-values obtained from field tests under different effective overburden pressures are corrected to a standard effective overburden pressure.

Overburden correction adjusts the measured N- values to what they would have been if the vertical effective stress, σ_v' was 100 Kpa (2000lb/ft^2). The corrected value is,

$$(N_1)_{60} = \frac{N_{60}\sqrt{2000}}{\sigma_v'} \quad \ldots\ldots\ldots\ldots\ldots\ldots\ldots\ldots (5.5)$$

Where,

$(N_1)_{60}$ = SPT N value corrected for field procedures and overburden stress,

N_{60} = SPT N-value corrected for field procedures

σ_v' = vertical effective stress at the test location (KPa or lb/ft^2)

The corrected values of SPT for all three boreholes are shown in Appendix IV.

5.5 Correlation between Shear Wave Velocity and SPT Index

Seed et al. (1986) suggested that the shear velocity is approximately,

$V_s = C_1 N_{60}^{0.17} z^{0.2} F_1 F_2$ (m/s)

Where,

C_1 = empirical constant; Seed et al. (1986) suggested 69

z = depth in soil where blow count N_{60} is taken

F_1 = age factor

= 1 for Holocene age (alluvial deposits)

= 1.3 for Pleistocene age (diluvial deposits)

F_2 = soil factor as follows:

Table 5.5: Values of Soil factor (F_2) for different type of soil

	Clay	Fine Sand	Med Sand	Coarse Sand	Sand & Gravel	Gravel
F_2	1.0	1.09	1.07	1.11	1.15	1.45

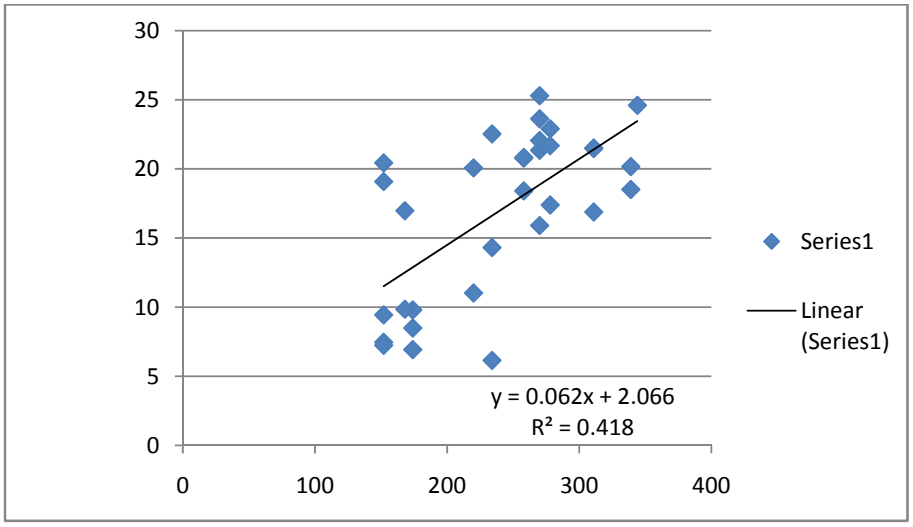

Fig. 5.1: ***Correlation between SPT and Shear wave velocity***

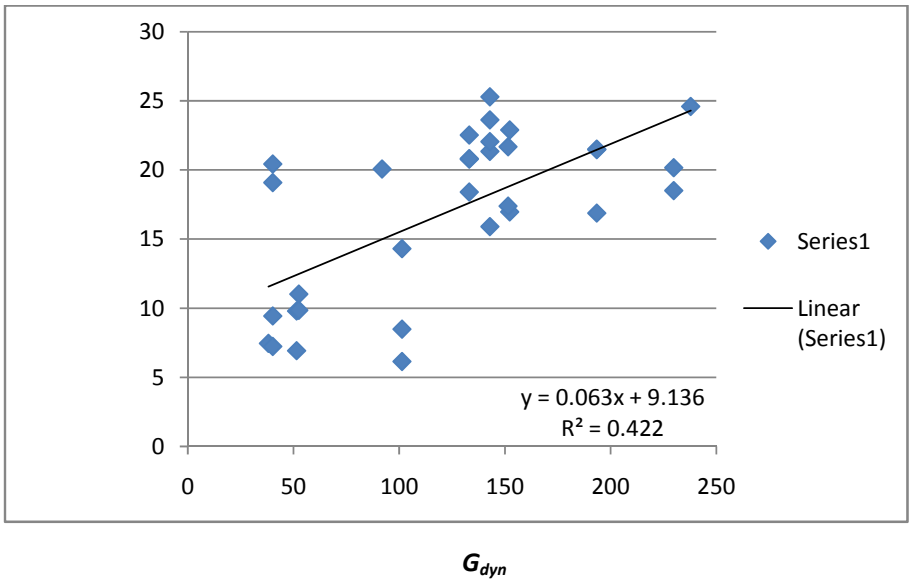

Fig. 5.2: ***Correlation between SPT and Dynamic Shear Modulus***

5.6 Results:

The graph shows moderate correlation between SPT-index and Shear wave velocity and between SPT-index and Dynamic Shear Modulus. Correlation coefficient for SPT versus V_s is 0.418 and for SPT versus G_{dyn}, it is 0.422.

CHAPTER SIX

ASSESSMENT OF LIQUEFACTION POTENTIAL

6.1 Introduction

Evaluating the liquefaction resistance of soils is an important step in the engineering design of new structures and the retrofit of existing structures in earthquake-prone regions. Amongst several types of evaluating procedures that have evolved over the last three decades, the well known "*simplified procedure*" has been widely used. The simplified procedure was originally developed by Seed and Idriss (1971) using blow counts from the Standard Penetration Test (SPT) correlated with a parameter representing the seismic loading on the soil, called the *cyclic stress ratio*. Over the years, the simplified procedure has been modified and updated with additional data, and has become the most commonly used way to assess the potential for granular soils to liquefy (Robertson and Wride, 1998; Harder, 1997).

Geological and historical records suggest that earthquake can cause widespread destruction to cities established in young alluvial valleys. For example wide spread liquefaction had occurred in Kathmandu during the 1934 earthquake. A combination of factors such as presence of active seismic faults, young loose alluvium and shallow ground water could result in liquefaction. Fine sands and non-plastic or plastic silts under saturated condition can liquefy under dynamic loading. Even some gravelly soils are vulnerable to liquefaction if they are in confined condition, which prevents rapid dissipation of seismically induced pore pressure. In general, water saturated cohesion-less material containing less than 20% (by weight) of fines are considered susceptible to liquefaction.

6.2 Liquefaction

If saturated cohesion less materials are subjected to earthquake ground vibrations, the resulting tendency to compact must be accompanied by an increase in pore water pressure in the soil and a resulting movement of water

from voids. Water is thus caused to flow upward to the ground surface, where it emerges in the form of mud spouts or sand boils. The development of high pore-water pressures due to ground vibrations and the resulting upward flow of water may turn sand into a 'quick' or liquefied condition. If liquefaction occurs in or under a slopping soil mass, the entire mass will flow or translate laterally to the unsupported side in a phenomenon termed a flow slide. Such slides also develop in loose, saturated, cohesion-less materials during earthquakes.

Liquefaction occurs when the structure of loose, saturated sand breaks due to some rapidly applied loading. As the structure breaks down, the loosely-packed individual soil particles attempt to move into a denser configuration. In an earthquake, however, there is not enough time for the water in the pores of the soil to be squeezed out. Instead the water is 'trapped' and prevents the soil particles from moving closer together. This is accompanied by an increase in water pressure which reduces the contact forces between the individual soil particles, thereby softening and weakening the soil deposit.

The forces are small because of the high water pressure. In an extreme case, the pore-water pressure may become so high that many of the soil particles loose contact with each other. In such cases the soil will have very little strength and will behave more liquid than a solid hence, the name '*liquefaction*'. Sometimes the shear strength falls to nearly zero, while other times it only drops to a lower-than-normal value. In either case, liquefaction can lead to many kinds of failures, so its evaluation is one of the most important aspects of geotechnical earthquake engineering.

There are two types of liquefaction:

- *Flow liquefaction* occurs when the static shear stresses in the soil exceed the shear strength of the liquefied soil. This usually leads to large and sudden shear movements in the soil.
- *Cyclic mobility* occurs when the static shear stresses are slightly less than the liquefied shear strength, but the static plus dynamic stresses are greater than the liquefied shear strength. This produces incremental shear movements that are generally not as dramatic as flow liquefaction, but still can be a source of significant damage.

6.3 Liquefaction Assessment

Liquefaction potential is generally assessed using the "simplified procedure", which has now become a standard practice for evaluating liquefaction potential in many countries. Calculation, or estimation, of two variables is required for evaluation of liquefaction resistance of soils:

- The seismic demand on a soil layer, expressed in terms of cyclic stress ratio (CSR), and
- The capacity of the soil to resist liquefaction, expressed in terms of cyclic resistance ratio (CRR).

6.3.1 SPT:

Criteria for evaluation of liquefaction resistance base on the SPT have been rather robust over the years. Those criteria are largely embodied in the CSR versus $(N_1)_{60}$ plot.

According to Seed et al. (1986), the critical value of field SPT at which the soil layer is liquefiable is given by;

$$N_{crit} = N\{1 + 0.125\,(d_s - 3) - 0.05\,(d_w - 2)\} \quad \text{(6.1)}$$

Where,

d_s is depth of sand layer

d_w is depth of water table

N is a function of earthquake shaking intensity as follows:

Relative liquefaction potential is generally assessed on the basis of some well known criteria given below:

Table 6.1: Relative liquefaction susceptibility of natural sediments as function of groundwater table depth, (Youd T.L., 1995)

Groundwater table	Liquefaction susceptibility
Less than 3m	Very high

3m to 10 m	High
10 m to 15 m	Moderate
More than15 m	Low to very low

Table 6.2: Relative liquefaction susceptibility of natural sediments as function of SPT (N) values (Seed et al, 1985)

SPT (N) value	**Potential damage by liquefaction**
0 -20	High
20 – 30	Intermediate
More than 30	No significant damage

6.4 Evaluation of CSR:

Seed and Idriss (1971) proposed the following equation for calculation of the cyclic stress ratio:

$$CSR = \frac{\tau_{av}}{\sigma_v'} = 0.65\left(\frac{a_{max}}{g}\right)\left(\frac{\sigma_v}{\sigma_v'}\right)r_d \qquad \text{..... (6.2)}$$

Where a_{max} is the peak horizontal acceleration at the ground surface generated by the earthquake, g is the acceleration due to gravity, σ_v and σ_v' are total and effective overburden pressure at the depth of potentially liquefiable layer respectively, τ_{av} is average cyclic stress generated by earthquake. The latter coefficient accounts for the flexibility of the soil profile.

The stress reduction coefficient r_d is determined as follows;

r_d =1.0 - 0.0076 Z for Z≤ 9.15 m

r_d =1.174 - 0.0267 Z for 9.15 < Z ≤ 23 m

r_d = 0.744 – 0.008 Z for 23 < Z ≤ 30 m

r_d = 0.5 for Z > 30m

6.5 Liquefaction Resistance Based on Shear Wave Velocity

Small-strain shear wave velocity, V_s, measurements provide a promising alternative, or supplement, to the penetration-based approach for the assessment of liquefaction resistance. The use of V_s as an index of liquefaction resistance is soundly based because both V_s and liquefaction resistance are similarly influenced by many of the same factors (e.g., void ratio, state of stress, stress history, and geologic age).

The advantages of the shear wave velocity-based method were pointed out by many researchers (Andrus and Stokoe, 2000; Rauch *et al.* 2000), and this method can provide a promising alternative and supplementary means of liquefaction assessment. Over the past 20 years, numerous studies have been conducted to investigate the relationship between V_s and liquefaction resistance. Excellent reviews of these proposed V_s-based procedures were provided by Andrus *et al.* (1999) and Andrus and Stokoe (2000).

Some advantages of using Shear Wave Velocity are:

- Measurements are possible for soils that are difficult to penetrate with CPT and SPT to extract undisturbed samples, such as gravelly soils, and at sites where borings or soundings may not be permitted such as capped landfills.
- Measurements can be performed in small laboratory specimens allowing direct comparisons between measured laboratory and field behavior.
- Shear Wave Velocities are directly related to small strain shear modulus, G_{max}, an elastic parameter required in analytical procedures for estimating dynamic shear strain in soils.
- For large magnitude earthquake and long durations of shaking, the cyclic strain needed for liquefaction decreases and approaches the threshold strain in sand (≈0.02%). Thus making it possible to conduct analytical evaluation of liquefaction using G_{max} and V_s as basic parameter (Dobry et al. 1981, seed et al. 1983).

Limitations of using V_s to evaluate liquefaction resistance are:

- Seismic wave velocity measurements are made at small strains, where as pore-water pressure buildup and the onset of liquefaction are medium- to large-strain phenomena.
- Seismic testing does not provide samples for classification of soils and identification of non liquefiable soft clay-rich soils.
- Thin, low V_s strata may not be detected if the measurement interval is too large.

Stokoe et al (1988b) correlated V_s of the liquefiable sand layer with a_{max} estimated for reference soil site. He noted that,

- The higher the V_s, less likely the site are liquefiable for given a_{max}.
- The greater thickness of the liquefiable sand layer, the less likely the site is liquefiable for given V_s.
- The greater the depth of liquefiable sand layer that slightly more likely the site is liquefiable for given V_s.

6.6 Stress-Corrected Shear Wave Velocity

Following the traditional procedures for correcting SPT blow count to account for overburden stress, one can correct V_s to a reference stress by (Sykora, 1987; Robertson et al., 1992):

$$V_{s1} = V_s \left(\frac{P_a}{\sigma_v'}\right)^{0.25} \quad \text{..... (6.3)}$$

Where,

V_{s1} is the overburden stress-corrected shear wave velocity

P_a is a reference stress, 100 KPa of about atmospheric pressure

σ_v' is initial effective overburden stress in KPa.

While using equation (6.3), it is implicitly assumed that the initial effective horizontal stress, σ_h' is a constant factor of the effective overburden stress. The factor, generally referred to as *K'*, is assumed to be approximately 0.5 at sites, where liquefaction has occurred.

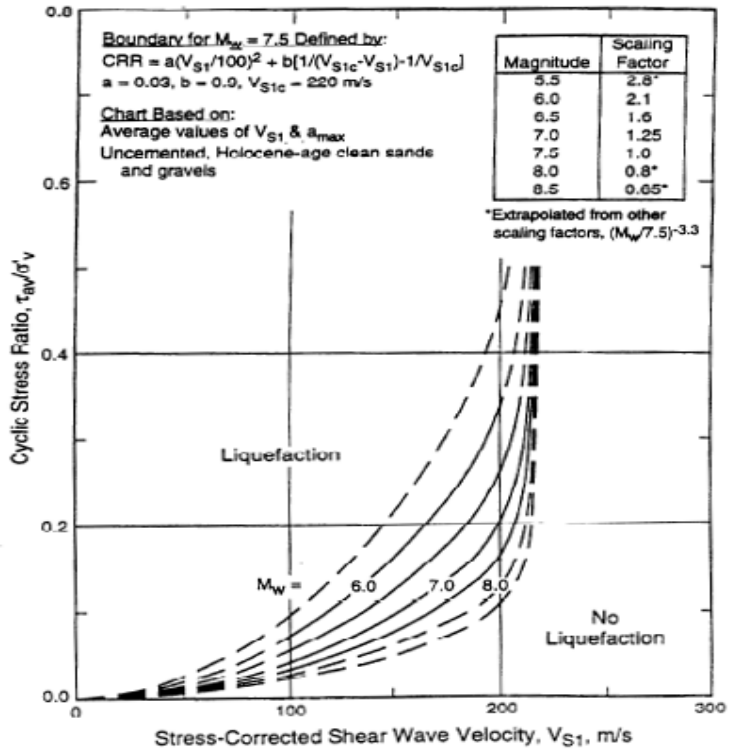

Fig. 6.1: ***Recommended Chart Based on V_{s1} and CSR for Evaluation of Liquefaction Potential of Uncemented Clean Sands and Gravels of Holocene Age.***

Symbol of particular layer	Depth m	σ_v (KN/m^2)	σ_v' (KN/m^2)	Thickness assumed (z)	σ_v/σ_v'	r_d	Magnitude Richter Scale	a_{max}/g	CSR	% of fines	V_s	V_{s1}
BH3-1	2--3.5	50.274	40.474	1.5	1.2421	0.9885	6	0.1525	0.1217	3.9	152	190.57
							6.5	0.2187	0.1745			
							7	0.3136	0.2503			
							7.5	0.4496	0.3588			
							8	0.6448	0.5146			
							8.5	0.9245	0.7379			
BH3-2	4.5--7	118.482	69.482	2.5	1.7052	0.9809	6	0.1525	0.1658	13.2	152	166.49
							6.5	0.2187	0.2378			
							7	0.3136	0.3409			
							7.5	0.4496	0.4888			
							8	0.6448	0.7010			
							8.5	0.9245	1.0051			

Table 6.3: Calculation of Cyclic Stress Ratio and Stress corrected Shear wave Velocity (for Borehole – 3)

Symbol of particular layer	Depth m	σ_v (KN/m^2)	σ_v' (KN/m^2)	Thickness assumed (z)	σ_v/σ_v'	r_d	Magnitude Richter Scale	$a_{max/g}$	CSR	% of fines	V_s	V_{s1}
BH5-1	1--3	49.98	49.98	3	1.0000	0.9771	6	0.1525	0.10	1.6	174	206.94
							6.5	0.2187	0.14			
							7	0.3136	0.20			
							7.5	0.4496	0.29			
							8	0.6448	0.41			
							8.5	0.9245	0.59			
BH5-2	4--6	104.37	82.81	3	1.2604	0.9541	6	0.1525	0.12	3.4	234	245.29
							6.5	0.2187	0.17			
							7	0.3136	0.25			
							7.5	0.4496	0.35			
							8	0.6448	0.50			
							8.5	0.9245	0.72			
BH5-3	14--20	378.77	220.01	6	1.7216	1.0138	6	0.1525	0.17	2.8	203	166.68
							6.5	0.2187	0.24			
							7	0.3136	0.35			
							7.5	0.4496	0.51			
							8	0.6448	0.73			
							8.5	0.9245	1.04			

Table 6.4: Calculation of Cyclic Stress Ratio and Stress corrected Shear wave Velocity (for Borehole – 5)

Symbol of particular layer	Depth m	σ_v (KN/m^2)	σ_v' (KN/m^2)	Thickness assumed (z)	σ_v/σ_v'	r_d	Magnitude Richter Scale	$a_{max/g}$	CSR	% of fines	V_s	V_{s1}
BH8-1	4--5	92.708	75.068	1	1.2349	0.992	6	0.1525	0.12	1.3	220	236.3518
							6.5	0.2187	0.17			
							7	0.3136	0.24			
							7.5	0.4496	0.35			
							8	0.6448	0.51			
							8.5	0.9245	0.73			
BH8-2	5--9	166.698	109.858	4	1.5173	0.969	6	0.1525	0.14	3.75	168	164.0973
							6.5	0.2187	0.20			
							7	0.3136	0.29			
							7.5	0.4496	0.42			
							8	0.6448	0.61			
							8.5	0.9245	0.88			

Table 6.5: Calculation of Cyclic Stress Ratio and Stress corrected Shear wave Velocity (for Borehole – 8)

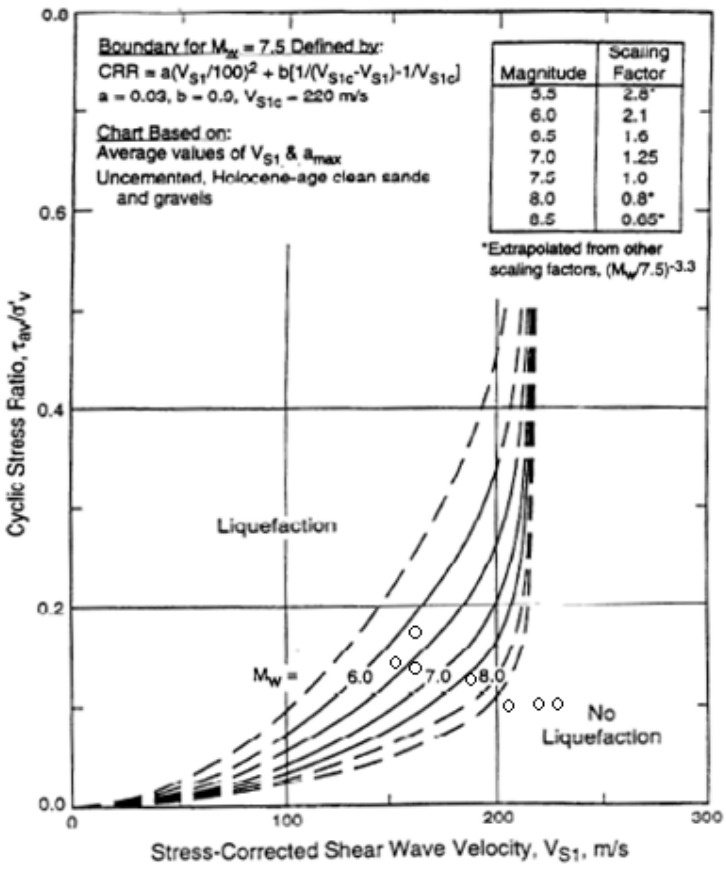

Fig. 6.2: Comparison of Liquefaction Assessment Chart Based on V_{s1} and CSR for Evaluation of Liquefaction Potential for Earthquake of Magnitude - 6

Results:

Symbol of the layer	CSR	V_{S1}	Remarks
BH3-1	0.121	190.57	Not Liquefiable
BH3-2	0.165	166.49	Not Liquefiable
BH5-1	0.10	206.9	Not Liquefiable
BH5-2	0.12	245.29	Not Liquefiable
BH5-3	0.17	166.68	Not Liquefiable
BH8-1	0.12	236.35	Not Liquefiable
BH8-2	0.14	164.09	Not Liquefiable

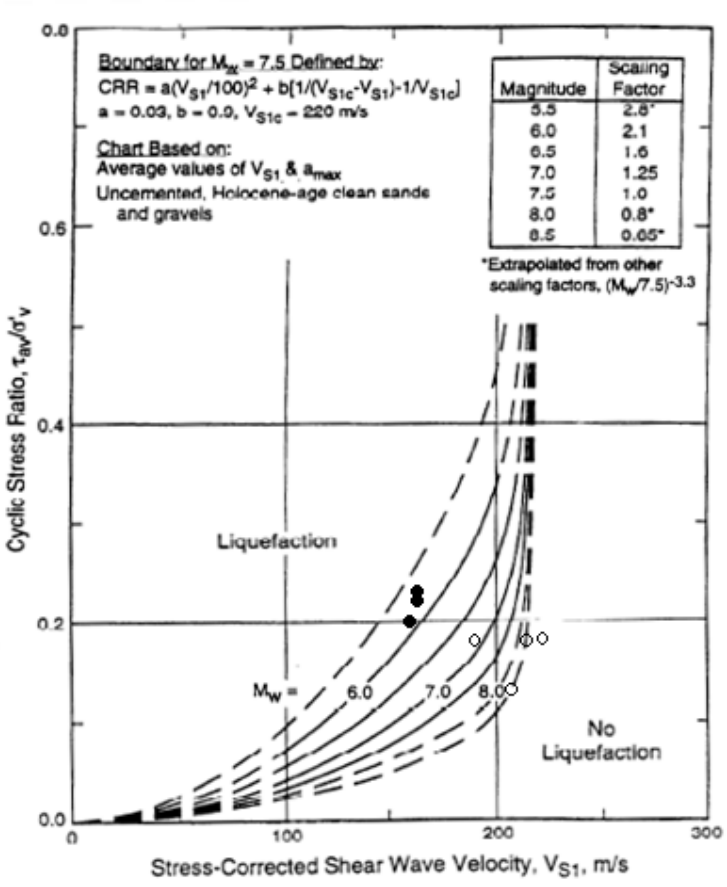

Fig. 6.3: Comparison of Liquefaction Assessment Chart Based on V_{s1} and CSR for Evaluation of Liquefaction Potential for Earthquake of Magnitude – 6.5

Results:

Symbol of the layer	CSR	V_{S1}	Remarks
BH3-1	0.174	190.57	Not Liquefiable
BH3-2	0.237	166.49	Liquefiable
BH5-1	0.14	206.9	Not Liquefiable
BH5-2	0.17	245.29	Not Liquefiable
BH5-3	0.24	166.68	Liquefiable
BH8-1	0.17	236.35	Not Liquefiable
BH8-2	0.20	164.09	Liquefiable

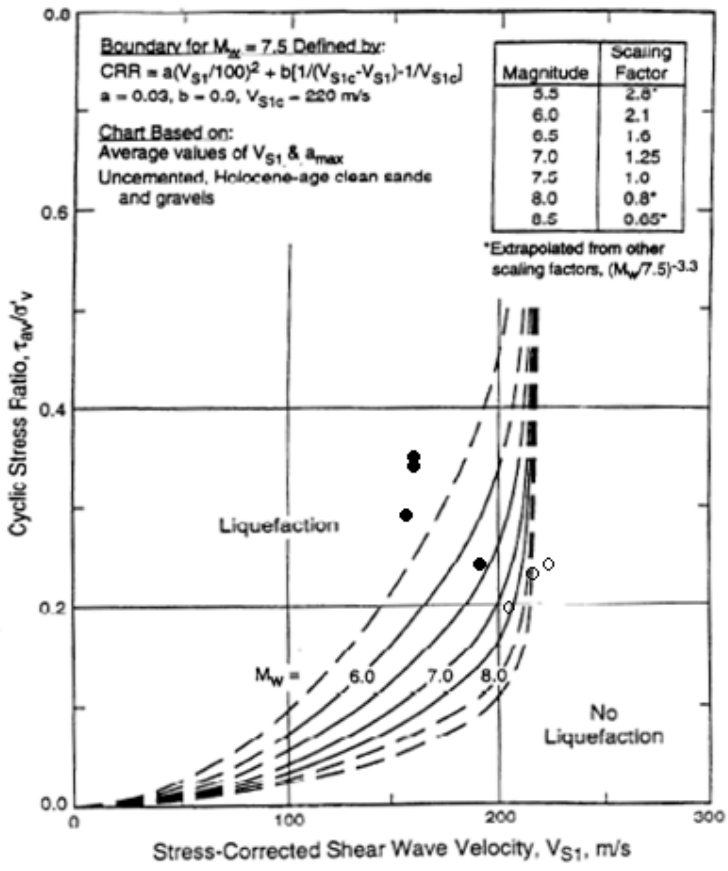

Fig. 6.4: Comparison of Liquefaction Assessment Chart Based on V_{s1} and CSR for Evaluation of Liquefaction Potential for Earthquake of Magnitude - 7

Results:

Symbol of the layer	CSR	V_{S1}	Remarks
BH3-1	0.25	190.57	Liquefiable
BH3-2	0.34	166.49	Liquefiable
BH5-1	0.20	206.9	Not Liquefiable
BH5-2	0.25	245.29	Not Liquefiable
BH5-3	0.35	166.68	Liquefiable
BH8-1	0.24	236.35	Not Liquefiable
BH8-2	0.29	164.09	Liquefiable

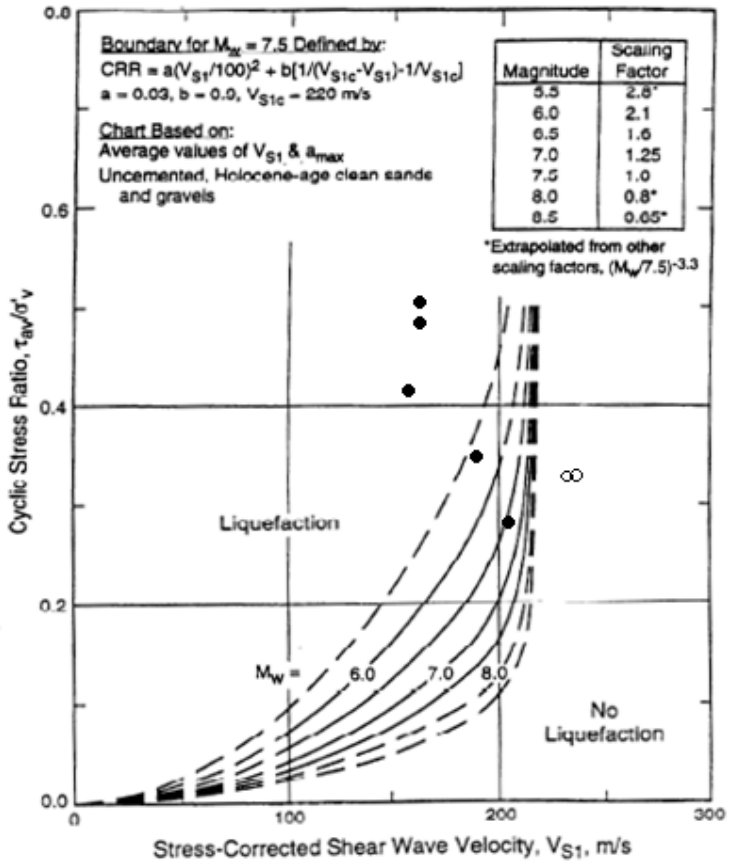

Fig. 6.5: Comparison of Liquefaction Assessment Chart Based on V_{s1} and CSR for Evaluation of Liquefaction Potential for Earthquake of Magnitude – 7.5

Results:

Symbol of the layer	CSR	V_{S1}	Remarks
BH3-1	0.35	190.57	Liquefiable
BH3-2	0.48	166.49	Liquefiable
BH5-1	0.29	206.9	Liquefiable
BH5-2	0.35	245.29	Not Liquefiable
BH5-3	0.51	166.68	Liquefiable
BH8-1	0.35	236.35	Not Liquefiable
BH8-2	0.42	164.09	Liquefiable

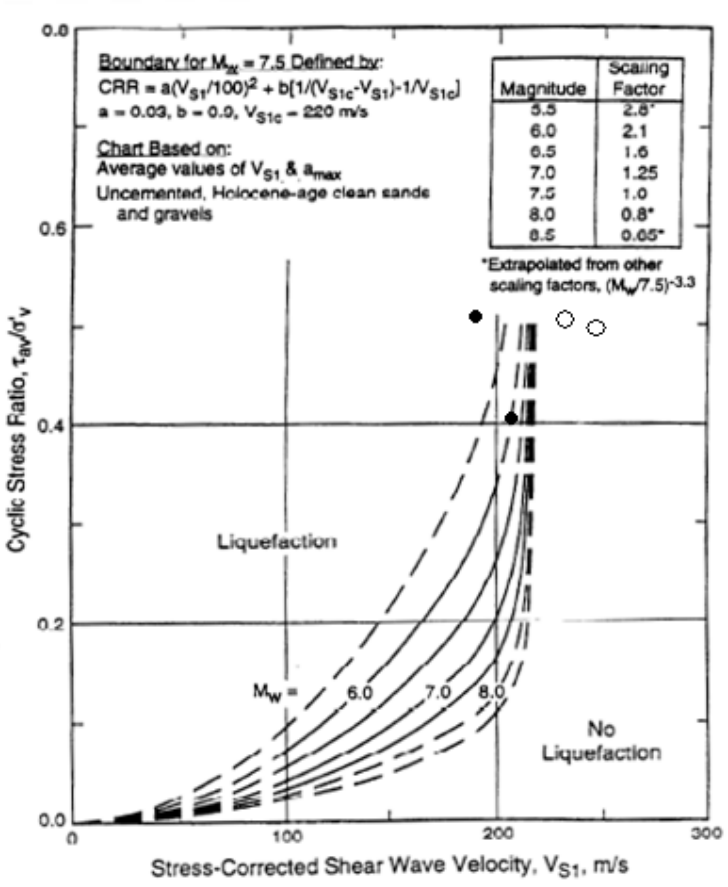

Fig. 6.6: Comparison of Liquefaction Assessment Chart Based on V_{s1} and CSR for Evaluation of Liquefaction Potential for Earthquake of Magnitude - 8

Results:

Symbol of the layer	CSR	V_{S1}	Remarks
BH3-1	0.51	190.57	Liquefiable
BH3-2	0.70	166.49	----
BH5-1	0.41	206.9	Liquefiable
BH5-2	0.50	245.29	Not Liquefiable
BH5-3	0.73	166.68	----
BH8-1	0.51	236.35	Not Liquefiable
BH8-2	0.61	164.09	----

6.7 Cyclic Resistance Ratio (CRR)

The value of CSR separating liquefaction and non-liquefaction occurrences for a given V_s, or corrected blow count, is called the *cyclic resistance ratio*.

Andrus and Stokoe (1997) proposed the following relationship between *CRR* and V_{s1}:

$$CRR = \left\{ a\left(\frac{V_{S1}}{100}\right)^2 + b\left[\left(\frac{1}{V'_{S1} - V_{S1}}\right) - \frac{1}{V'_{S1}}\right]\right\} MSF \quad \text{..... (6.4)}$$

Where,

V'_{s1} is the limiting upper value of V_{s1} for liquefaction occurrence whose values depending upon fine contents (FC) are :

V'_{s1}= 200 m/s for FC ≥ 35%, V'_{s1}=208 m/s for FC = 20 % and V'_{s1}= 215 m/s for FC ≤ 5 %; a and b are curve fitting parameters and *MSF* is the magnitude scaling factor.

The first term of the last equation is based on a modified relationship between V_{s1} and CSR for constant average cyclic shear strain suggested by R. Dobry (personal communication to R. D. Andrus, 1996; Andrus and Stokoe, 1997). The second term is a hyperbola with a small value at low values of V_{s1}, and a very large value as V_{s1} approaches V'_{s1}.

The magnitude scaling factor, which accounts for the effect of earthquake magnitude on CRR, can be expressed by;

$$MSF = \left(\frac{M_w}{7.5}\right)^n \quad \text{..... (6.5)}$$

Where n is an exponent

The lower bound for the range of magnitude scaling factors recommended by the 1996 National Center for Earthquake Engineering Research (NCEER) Workshop on Evaluation of Liquefaction Resistance of Soils (Youd et al. 1997) is defined by the last equation with n = -2.56 (Idriss, 1995).

Table 6.6 shows various MSF values given by various researchers.

Table 6.6: Magnitude Scaling Factor Values Defined by Various Investigators (Youd & Noble 1997a)

Magnitude Scaling Factor Values Defined by Various Investigators (Youd and Noble 1997a)									
Magnitude, M	**Seed and Idriss (1982)**	**Idriss***	**Ambraseys (1988)**	**Arango (1996)**		**Andrus and Stokoe (1997)**	**Youd and Noble (1997b)**		
				Distance Based	**Energy Based**		**P_L < 20%**	**P_L < 32%**	**P_L < 50%**
5.50	1.43	2.20	2.86	3.00	2.20	2.80	2.86	3.42	4.44
6.00	1.32	1.76	2.20	2.00	1.65	2.10	1.93	2.35	2.92
6.50	1.19	1.44	1.69	1.60	1.40	1.60	1.34	1.66	1.99
7.00	1.08	1.19	1.30	1.25	1.10	1.25	1.00	1.20	1.39
7.50	1.00	1.00	1.00	1.00	1.00	1.00	-	-	1.00
8.00	0.94	0.84	0.67	0.75	0.85	0.8?	-	-	0.73
8.50	0.89	0.72	0.44	-	-	0.65?	-	-	0.56
Note: ? = Very uncertain values									
*1995 Seed Memorial Lecture, University of California at Berkeley (I.M. Idriss, personal communication to T. L. Youd, 1997									

6.8 Factor of Safety

A common way to quantify the hazard for liquefaction is in terms of a factor of safety, *FS*. The *FS* against liquefaction can be defined by,

$$FS = \frac{CRR}{CSR} \quad \text{..... (6.6)}$$

Liquefaction is predicted to occur when $FS \leq 1$, and liquefaction is predicted not to occur when $FS > 1$. The acceptable value of *FS* for a particular site will depend on several factors, including the acceptable level of risk for the project, the extent and accuracy of seismic measurements, the availability of other site information, and the conservatism in determining the design earthquake magnitude and the expected value of a_{max}.

Symbol of particular layer	Depth m	Magnitude Richter Scale	$a_{max/g}$	CSR	V_s	V_{s1}	V'_{s1}	MSF	CRR	FS	Remarks
BH3-1	2 -- 3.5	6	0.1525	0.1217	152	190.5678	215	2.1	0.381098	3.131109	Not liquefiable
		6.5	0.2187	0.1745				1.6	0.29036	1.663489	Not liquefiable
		7	0.3136	0.2503				1.25	0.226844	0.906322	Liquefiable
		7.5	0.4496	0.3588				1	0.181475	0.505734	Liquefiable
		8	0.6448	0.5146				0.8	0.14518	0.282107	Liquefiable
		8.5	0.9245033	0.7379				0.65	0.117959	0.159865	Liquefiable
BH3-2	4.5 -- 7	6	0.1525	0.1658	152	166.4852	208	2.1	0.241421	1.456122	Not liquefiable
		6.5	0.2187	0.2378				1.6	0.18394	0.773605	Liquefiable
		7	0.3136	0.3409				1.25	0.143703	0.421485	Liquefiable
		7.5	0.4496	0.4888				1	0.114962	0.235192	Liquefiable
		8	0.6448	0.701				0.8	0.09197	0.131194	Liquefiable
		8.5	0.9245033	1.0051				0.65	0.074725	0.074345	Liquefiable

Table 6.7: Calculation of Cyclic Resistance Ratio and Factor of Safety

Symbol of particular layer	Depth m	Magnitude Richter Scale	$a_{max/g}$	CSR	V_s	V_{s1}	V'_{s1}	MSF	CRR	FS	Remarks
BH5-1	1 -- 3	6	0.1525	0.0969	174	206.943	215	1.77	0.759	7.837	Not Liquefiable
		6.5	0.2187	0.1389				1.442	0.6184	4.4522	Not Liquefiable
		7	0.3136	0.1992				1.193	0.5115	2.5684	Not Liquefiable
		7.5	0.4496	0.2855				1	0.4287	1.5014	Not Liquefiable
		8	0.6448	0.4095				0.848	0.3634	0.8875	Liquefiable
		8.5	0.9245	0.5871				0.726	0.3112	0.53	Liquefiable
BH5-2	4 -- 6	6	0.1525	0.1192	234	245.299	215	1.77	0.0477	0.4002	Liquefiable
		6.5	0.2187	0.1709				1.442	0.0389	0.2273	Liquefiable
		7	0.3136	0.2451				1.193	0.0321	0.1311	Liquefiable
		7.5	0.4496	0.3514				1	0.0269	0.0767	Liquefiable
		8	0.6448	0.504				0.848	0.0228	0.0453	Liquefiable
		8.5	0.9245	0.7226				0.726	0.0196	0.0271	Liquefiable
BH5-3	14 -- 20	6	0.1525	0.173	203	166.681	215	1.77	0.1878	1.0852	Not Liquefiable
		6.5	0.2187	0.2481				1.442	0.153	0.6165	Liquefiable
		7	0.3136	0.3558				1.193	0.1265	0.3557	Liquefiable
		7.5	0.4496	0.5101				1	0.106	0.2079	Liquefiable
		8	0.6448	0.7315				0.848	0.0899	0.1229	Liquefiable
		8.5	0.9245	1.0488				0.726	0.077	0.0734	Liquefiable

Table 6.8: Calculation of Cyclic Resistance Ratio and Factor of Safety

Symbol of particular layer	Depth m	Magnitude Richter Scale	$a_{max/g}$	CSR	V_s	V_{s1}	V'_{s1}	MSF	CRR	FS	Remarks
BH8-2	5 -- 9	6.0000	0.1525	0.1458	168	164.10	215	1.7705	0.1792	1.2289	Not liquefiable
		6.5000	0.2187	0.2091				1.4424	0.1460	0.6981	Liquefiable
		7.0000	0.3136	0.2999				1.1932	0.1208	0.4027	Liquefiable
		7.5000	0.4496	0.4300				1.0000	0.1012	0.2354	Liquefiable
		8.0000	0.6448	0.6166				0.8477	0.0858	0.1392	Liquefiable
		8.5000	0.9245	0.8841				0.7258	0.0735	0.0831	Liquefiable

Table 6.9: Calculation of Cyclic Resistance Ratio and Factor of Safety

6.9 Determination of the Peak Horizontal Acceleration

The intensity of ground shaking during an earthquake is often expressed in terms of peak acceleration, usually in units of 'g' where 1g = the acceleration of gravity (= 9.8 m/s^2). Peak ground acceleration (PGA) at a site depends upon earthquake magnitude and source to site distance which describes the attenuation relationship. There are a number of empirical attenuation models developed based on different amount of data of different quality measured from the earthquake occurred in the past in various regions of the world. Because of the differences in bedrock, these functions usually apply only to a certain geographic area.

Boore, et al. (1993) developed the following function for earthquakes in the western United States:

$$\log(a_{max/g}) = -0.038 + 0.216(M_w - 6) - 0.777 log R + 0.158 G_B + 0.254 G_C \quad \text{..... (6.7)}$$

$$R = \sqrt{d^2 + z_1^2}$$

Where,

$a_{max/g}$ = peak horizontal ground acceleration at the ground surface

M_w = moment magnitude

d = closest distances to fault trace (km)

z_1 = focal depth (km) (if unknown, 5 km is a conservative value)

G_B, G_C = empirical coefficients from Table below

Table 6.10: Coefficients G_B and G_C (Boore, et al. 1993)

Site Class	Shear Wave Velocity in Upper 30 m	G_B	G_C
A	>750 m/s	0	0
B	360 – 750 m/s	1	0
C	180 – 360 m/s	0	1

Toro, et al. (1995) has developed a different function for earthquakes in the central and eastern United States:

$$ln\ (a_{max/g}) = 2.20 + 0.81(M_w - 6) - 1.27lnR + 0.11max\ (ln\frac{R}{100}, 0) - 0.0021R$$

…… (6.8)

Where,

$(a_{max/g})$ = peak horizontal acceleration in bedrock

$R = \sqrt{d^2 + 9.3^2}$

d = closest distance to fault trace (km)

The fourth term in the equation (6.8) uses the greater of the two numbers in the parenthesis.

According to Kawashima et al. (1984) and Kawashima et al.(1986)

$lnPGA = 232.4 * 10(0.313 * M) * (R + 30)^{(-1.218)}$ …… (6.9)

Where *PGA* is in gal

According to Cornell et al. (1979)

$$LnPGA = 6.74 + 0.859 * M - 1.8 * \ln\ (R = 25)$$

Table 6.11: Calculation of Peak Ground Acceleration {Kawashima et al. (1984) and Kawashima et al. (1986)}

Source	Fault name	Fault type	Hypocen-tral Distance R (km)	Mean min. Magnitude M_w	Assumed M_{max}	PHA (981 gal)	ln PHA	PGA
MCT - 3.3	Gosain-kunda	Reverse	20	5	7.6	72.79	4.287	0.074
				6		149.6	5.008	0.152
				6.5		214.5	5.368	0.218
				7		307.6	5.729	0.313
				7.5		441.1	6.089	0.449
				8		632.5	6.449	0.644
				8.5		906.9	6.810	0.924

CHAPTER SEVEN

CONCLUSION AND RECOMMENDATION

7.1 Conclusions:

- Young Modulus (Edyn) ranges from 91- 672 MPa where most of the values are closer to 400 MPa.
- Dynamic Shear Modulus (Gdyn) ranges between 38 MPa to 238 MPa; most of the values are around 150 or less.
- Poisson's ratio ranges between 0.43 – 0.49.
    - Low value of Poisson's ratio is obtained for unsaturated material close to surface.
    - High value of Poisson's ratio indicates the liquid state of subsurface formation.
- Shear wave velocity ranges from 152 m/sec to 344 m/sec in all of the three bore holes.
- Predominant period and frequency of the ground vibration for borehole – 3 is 0.5 second and 1.96 Hz respectively; for Borehole – 5 is 0.355 second and 2.81 Hz; for Borehole – 8 is 0.463 second and 2.157 Hz.
- Considering the engineering bedrock at shear wave velocity 500 m/sec and density 2.2 gm/cm3 at a depth of 30 m and taking average weighted shear wave velocity of surface layer (0-30m) to be 263 m/s and average density to be 1.935 gm/cm3, ratio of amplification is 0.46.
- The soil is mainly fine to coarse sand with some intermittent layers of cohesive soils meaning that the soil is very liable to liquefaction.
- The layers susceptible to liquefaction are mostly less than 10m in depth except for Borehole-5, the layer between 14-20m in depth shows remarkable liquefaction potential.
- No layer is vulnerable to liquefaction at lesser magnitude earthquake (Mw = 6).

- Most of the layers poses liquefaction hazard for higher magnitude earthquake except for the layers BH5-2 and BH8-1, which shows no liquefaction vulnerability even at higher magnitude.

7.2 Recommendation

- The recorded field data indicate that there is high potential of liquefaction potential of the ground inside the premises of the Australian Embassy.
- Liquefaction assessment shows that soil at shallow depth (< 10 m) are most susceptible to liquefaction, therefore shallow foundation is not advisable.
- Deep foundation (such as pile foundation) is suggested.

References

Andrus, R. D., and Stokoe, K. H., II (1997), "Liquefaction Resistance Based on Shear Wave Velocity," *NCEER Workshop on Evaluation of Liquefaction Resistance of Soils*, Technical Report *NCEER-97-0022*, T. L., Youd and I. M. Idriss, Eds, 4-5 Jan. 1996, Nat. Ctr. for Earthquake Engrg., Res., Buffalo, NY, pp. 89 -128.

Andrus, R. D., and Stokoe, K. H. II (2000), "Liquefaction Resistance of Soils from Shear Wave Velocity," *Journal of Geotechnical and Geo-environment Engineering, ASCE,* 126, (11), pp. 1015-1025.

Andrus, R. D., Stokoe, K. H. II. and Chang, R. M. (1999), "Draft Guidelines for Evaluating Liquefaction Resistance Using Shear Wave Velocity Measurements and Simplified Procedures," *NISTIR 6277*, Nat. Institute of Standard and Technology, Gaithesburg, MD.

Arora, K. R. (2000), *Soil Mechanics and Foundation Engineering*, Fifth Edition, Standard Publishers Distributors, Nai Sarak, Delhi, pp. 773-768.

Basnet, S. (2008), "Geotechnical Investigation of Soil Foundation for Proposed Commercial Building, Patan, Nepal," (Unpublished) M. Sc. Dissertation, Tribhuvan University, Nepal.

Bolt, B. A. (1982), "Inside the Earth," San Fransisco, W. H. Freeman.

Boore, D. M., Joyner, W. B. and Fumal, T. E. (1993), "Estimation of Response Spectra and Peak Accelerations from Western North America Earthquakes," *An Interim Report, Open file Report 93-509,* U.S. Geological Survey, Reston, VA.

Bowles, J. E., (1968), *Foundation Analysis and Design*, McGraw Hill, New York.

Castanga, J. P., M. L. Bat Zle., R. L. Eastwood (1985), "Relationships between Compressional-Wave and Shear Wave Velocities in Elastic Silicate Rocks," *Geophysics*, v. 50, pp. 571-581.

Chaudhary, Anil K. (2007), "Dynamic Behaviour of Soil in Kathmandu Valley and its Application in Machine Foundation," (Unpublished) M. Sc. Dissertation, Tribhuvan University, Nepal.

Coduto, Donald P. (2006), *Geotechnical Engineering – Principles and Practices,* Prentice-Hall, INC., Upper Saddle River, New Jersey 07458, U.S.A., pp. 69-80; pp. 681-705.

Destegül Umut (2004), "Sensitivity Analysis of Soil Site Response Modelling in Seismic Microzonation for Lalitpur, Nepal," M. Sc. Dissertation, ITC., Enschede, The Netherlands.

Dobry, R., Stokoe, K. H., II, Ladd, R. S., and Youd, T. L. (1981), "Liquefaction Susceptibility from S-wave Velocity, " Proc., *In Situ Tests to Evaluate Liquefaction Susceptibility*, *ASCE Nat. Convention*, 27 Oct., St. Louis, MO.

Gorjainov, N. N. Ljachovickis F. M. (1979), "Seismiceskie metody v insenernoi geologii," Izdat. Nedra, Moskva.

Gurung, J. K. (1996), "Environmental Geological Survey along the Bagmati River, Metopolitan, Kathmandu city," Unpublished, M. Sc. Dissertation, T.U., Kirtipur, pp. 59.

Han, D., A. Nur, D. Morgan (1986), "Effects of porosity and clay content on wave velocities in sand stones," *Geophyciscs*, v. 51, 11, pp. 2093-2107.

Hornby, B. I., and W. F. Murphy (1987), "Vp/Vs in unconsolidated sands: Shear from Stoneley," *Geophysics*, v. 52, pp. 502-513.

JICA (Japan International Co-operation Agency) and MOHA (Ministry of Home Affairs)(2002), "The study on Earthquake Disaster Mitigation in the Kathmandu Valley, Kingdom of Nepal," *JICA & MOHA Dept. of Narcotics Control and Disaster Management.*

Kanai K. (1962), "On the predominant period of the Earthquake motions," *Bull. Of ERI.*, v.40.

Lambe, T. William, and Whitman, Robert V. (1969), *Soil Mechanics,* John Wiley, New York.

Lowrie, W. (1997), *Fundamental of Geophysics*, Cambridge University Press, United Kingdom, pp. 83-164.

Luna, R., and Jadi, H. (2000), "Determination of Dynamic Soil Properties Using Geophysical Methods," *Proceedings of the First International Conference on the Application of Geophysical and NDT Methodologies to Transportation Facilities and Infrastructure*, St. Louis, MO, December 2000.

Masuda, H. (1960), "Geophysical Exploration of the Dam Foundation," *Butsuritanko (Geophysical Exploration)*, v. 1300, pp. 25-35 (in Japanese).

Morgan, N. A. (1969), "Physical properties of marine sediments as related to seismic velocities," *Geophysics*, v. 34, 4, pp. 524-527.

Moribayashi, S., and Maruo, Y. (1980), "Basement topography of the Kathmandu Valley, Nepal - an application of gravitational method to the survey of a tectonic basin in the Himalayas," *Jour. Japan soc. Eng. Geol*. v. 21, pp. 30-37.

Nur, A., G. Simmons (1969), "The effect of saturation on velocity in low porosity rocks," *Earth and Planet, Sc. Letters,* Amsterdam, v.7, pp. 183-193.

Okamoto S. (1973), *Introduction to Earthquake Engineering*, University of Tokyo PRESS, Japan pp. 571.

Pickett, G. R. (1963), "Acoustic Character Log and their Application in Formation Evaluation," *Journal of Petroleum Technology*, 659-667.

Pomonis, A., Coburn, A.W. and Spence, J.S. (1993), "Seismic vulnerability, mitigation of human casualties and guidelines for low-cost earthquake resistant housing," STOP Disasters 12.

Pokhrel, R. M. (2006), "Detemination of Soil Dynamic Properties of Kathmandu Valley by Using Down the Hole Seismic Method," (Unpublished) M. Sc. Dissertation, Tribhuvan University, Nepal.

Reynolds J. M. (1997), *An introduction to Applied and Environmental Geophysics*, John Willey & Sons Ltd., Reynolds Geo-Sciences Ltd, UK,

Robertson, P. K., Woeller, D. J., and Finn, W. D. L. (1992), "Seismic Cone Penetration Test for Evaluating Liquefaction Potential Under Cyclic Loading," *Canadian Geotechnical Journal*, Ottawa, Canada, v. 29, pp. 686-695.

Rodriguez-Marek, A and J. D., and Bray (1999), "Characterization of Site Response," General Site Categories, Peer 1999/03.

Sah, R. B., Kirchner, M., Schauderna, H. and Schleich, H. H (1991), "Diatomites and their Fossils form Kathmandu Valley, Central Nepal," *München Geowiss. Abh.,* v. A19, pp. 57-64.

Sakai, H. (2001), "Stratigraphic Division and Sedimentary Facies of the Kathmandu Basin Group, Central Nepal," *Journal of Nepal Geological Society*, v. 25 (Sp. Issue), pp. 19-32.

Sakai, T., Gajurel, A.P, Tabata H., and Upreti B.N. (2001), " Small-amplitude lake-level fluctuations recorded in aggrading deltaic deposits of the Upper Pleistocene Thimi and Gokarna Formations, Kathmandu Valley," *Journal of Nepal Geological Society,* v.25 (Sp. Issue), pp. 19-31.

Schon, J. (1983), *Petrophysik*, Akademie Verlag Berlin and Ferd. Enke Verlag Stuttgart.

Schon, J. H. (1998). Physical Properties of Rocks: Fundamentals and Principles of Petrophysics, Second ed. ELSEVIER SCIENCE Ltd, The Boulevard, Langford Lane, Kidlington Oxford Ox 5 1GB, UK, Seismic Exploration, v, 18, pp. 583.

Seed, H. B., and Lee, K L. (1966), "Liquefaction of Saturated Sands during Cyclic Loading," *Journal of The soil Mechanics and Foundations Division*, *ASCE*, v. 92 (SM6), Proc. paper 4972, pp. 105-134.

Seed, H. B., and Idriss, I. M. (1971), "Simplified Procedure for Evaluating Soil Liquefaction Potential," *Journal of the Soil Mechanics and Foundations Division*, ASCE v. 107, No, SM9, pp. 1249-1274.

Seed, H. B., and Idriss, I. M (1982), "Ground Motions and Soil Liquefaction during Earthquakes," *In Engineering Monographs on Earthquake Criteria, Structural Design and Strong Motion Record,* Earthquake Engineering Research Institute.

Seed, H. Bolton, Tokimatsu, K., Harder, L.F., and Chung, Riley M. (1985), "Influence of SPT Procedures in Soil Liquefaction Resistance Evaluation,"*Journal of Geotechnical Engineering*, *ASCE,* 111(12), pp. 1425-1445.

Seed, H. B., and de Alba, (1986), " Use of SPT and CPT tests for Evaluating the Liquefaction Resistance of Sands, In Use of insitu Tests in Geotechnical Engineering," Edited by Clemence, S. P., American Society of Civil Engineers, Geotechnical Special Publicaiton 6, pp. 281-302.

Seed, H. B., M. P. Romo, et. al. (1987), "Relationships between Soil Conditions and Earthquake Ground Motions in Mexico City in the Earthquake of September 19, 1985," Earthquake Engineering Research center, College of Engineering, University of California, Berkeley, California.

Stocklin, J. (1980), "Geology of Nepal and its regional Frame," *Journal of the Geological Society of the London*, v. 37, pp. 1-34.

Stocklin, J., and Bhattarai, K. D. (1977), "Geology of the Kathmandu area and central Mahabharat range, Nepal Himalayas," *Report of Department of Mines and Geology/UNDP (unpublished)*, pp. 86.

Sykora, D. W. (1987), "Creation of a Database of Seismic Shear Wave Velocities for Correlation Analyis," *Geotech. Lab. Misc. Paper GL-87-26*, U.S. Army Engineer Waterways Exp. Station, Vicksburg, MS.

Terzaghi, K, and R.B. Peck (1967), *Soil Mechanics in Engineering Practice*, Second ed. John Wiley and Sons, New York.

Toro, G. R., Abrahamson, N.A., and Schneider, J.F. (1995), "Engineering Model of Strong Ground Motions from Earthquakes in the Central and Eastern United States," Earthquake Spectra.

Tosaja, C. and Nur, A. (1982), "Effects of Diagnosis and Clays on Compressional Velocities in Rocks," Geophysics, Res. Letters, v.9, No.1, pp. 5-8.

Wiegel Robert L., *Earthquake Engineering*, Prentice-Hall, INC., Englewood Cliffs, N.J., pp. 2-19; pp. 227-247.

Yoshida, M. and Gautam, P. (1988), "Magnetostratigraphy of Plio-Pleistocene Lacustrine Deposits in the Kathmandu Valley, Central Nepal," *Proc. Indian Natn. Sci. Acad*., 54, A3, pp. 410-417.

Yoshida, M., and Igarashi, Y. (1984), "Neogene to Quaternary Lacustrine Sediments in the Kathmandu Valley Nepal," *Journal of Nepal Geological Society*, 4, 7, pp. 3-100.

Youd, T. L., and Noble, S. K. (in press), "Magnitude Scaling Factors," *Proceedings, NCEE Workshop on Evaluation of Liquefaction Resistance*, held in Salt Lake City, Utah, T. L. Youd and I. M. Idriss, Eds., National Center for Earthquake Engineering Research, Buffalo, NY.

Youd et al. (1997), "Summary Report from the 1996 NCEER and 1998 NCEER/NSF Workshops on Evaluation of Liquefaction Resistance of Soils," *Technical Report NCEER*-97-0022, 4-5 Jan. 1996, Nat. Ctr. For Earthquake Engrg. Res., Buffalo, NY, pp. 1-40.

ANNEX – I

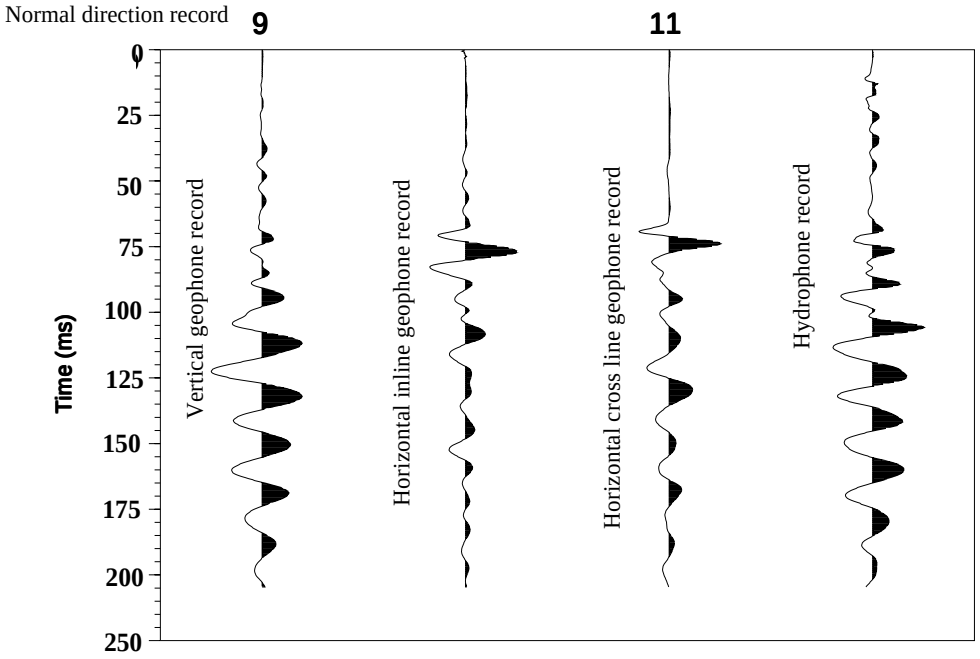

SPREAD: BORE-3A SHOT: 19 REC: MC019IFP.FPX

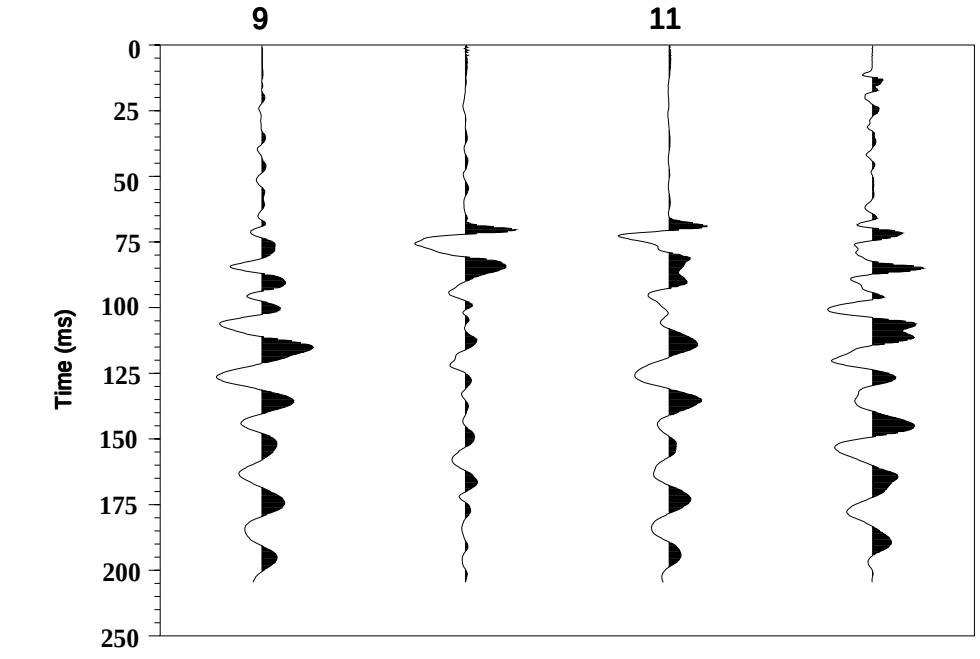

SPREAD: BORE-3A SHOT: 20 REC: MC020IFP.FPX

Seismogram from normal and reverse sources

ANNEX –II

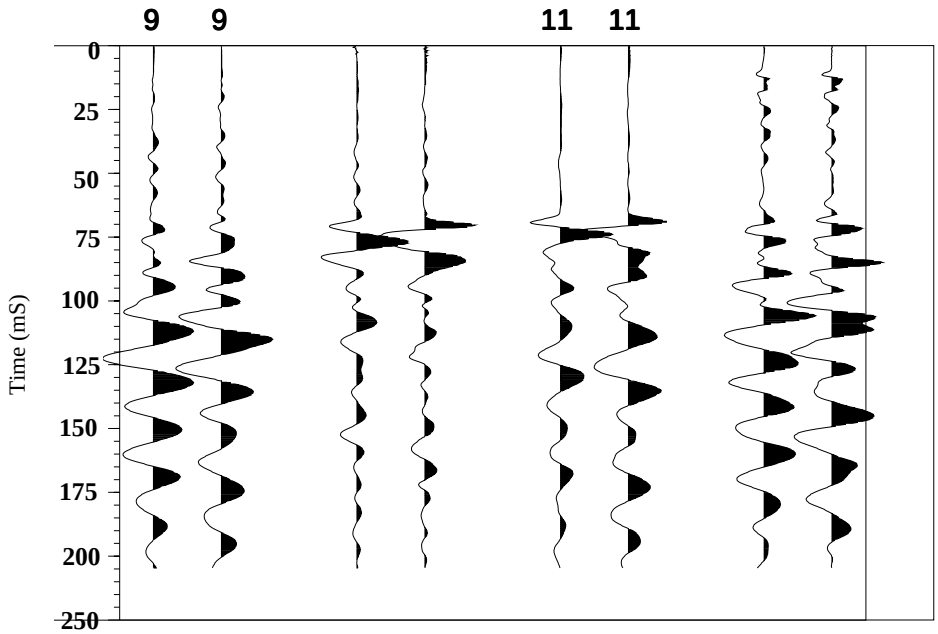

Note: P-wave have the same polarity and S-wave have different polarity

Layout of normal and reverse polarity records side by side

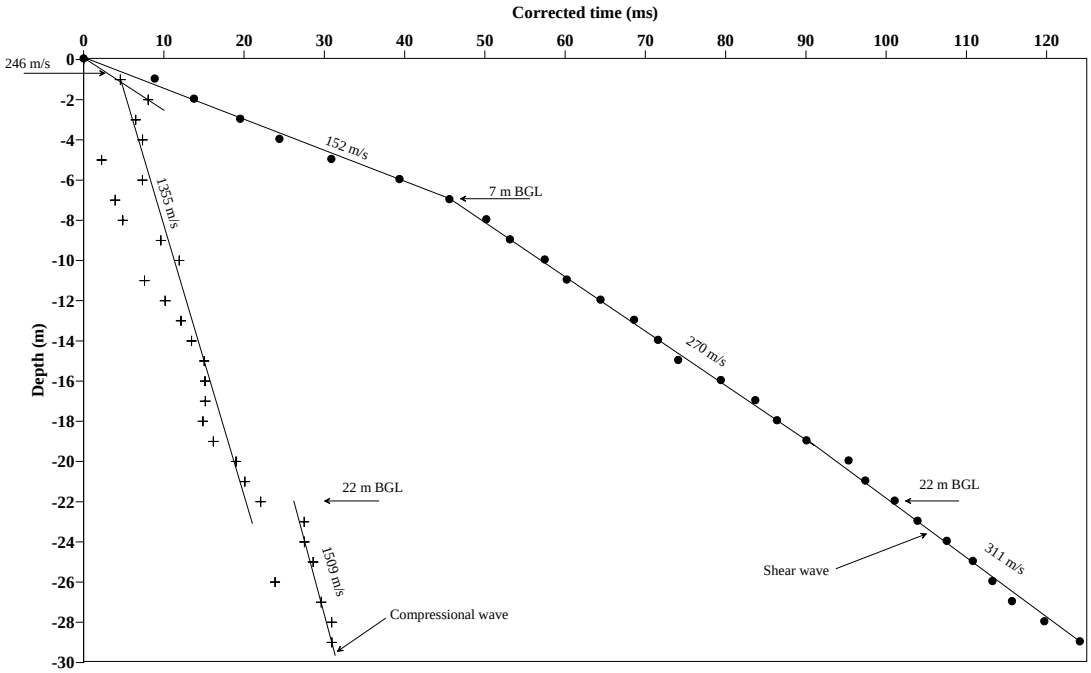

Compressional and shear waves travel time in Borehole No. 3

ANNEX – III

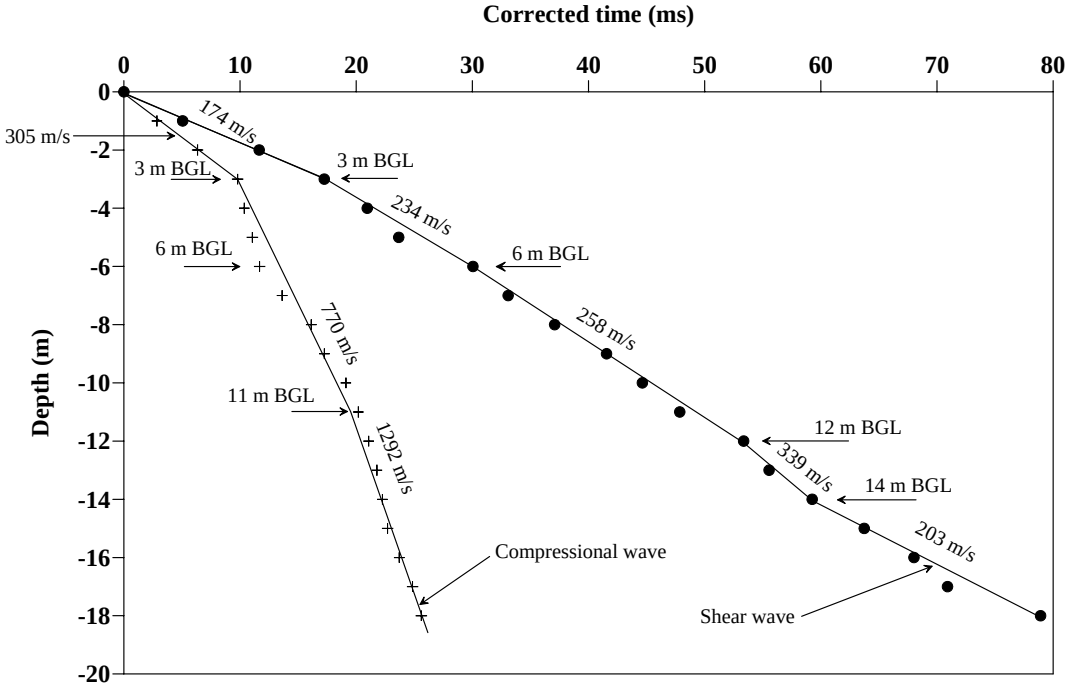

Compressional and sheared wave travel time in Borehole No. 5

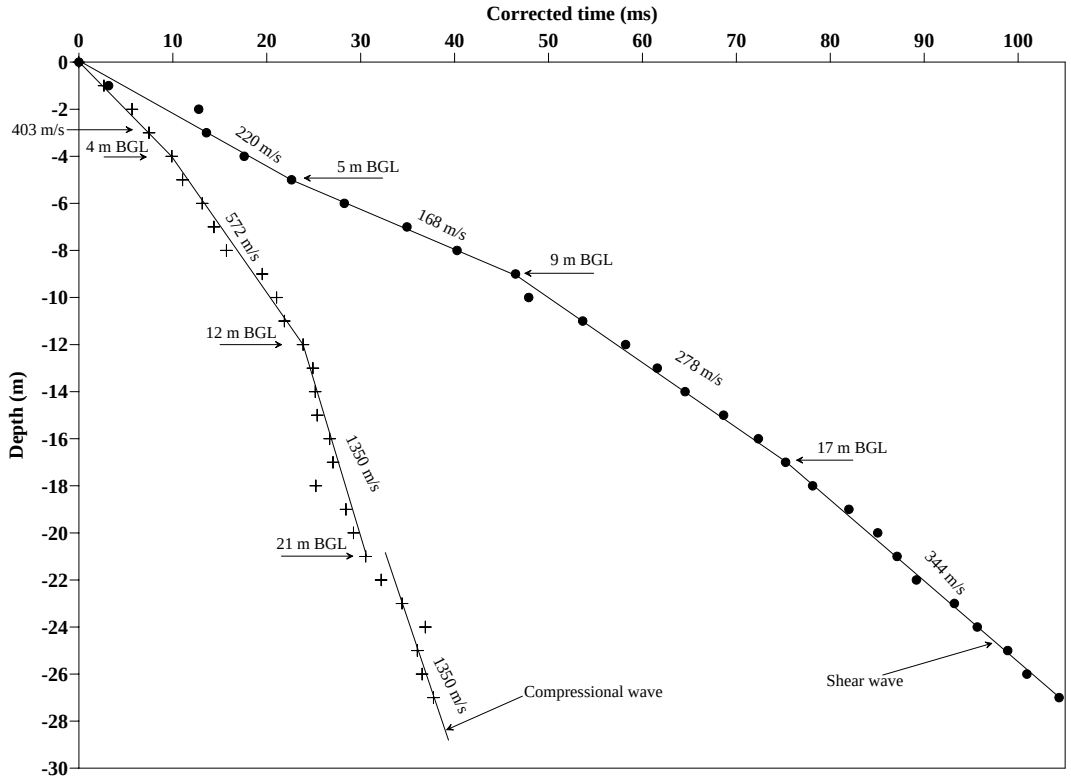

Compressional and shear wave travel time in Borehole No. 8

ANNEX - IV

Detail of the calculation of vertical travel time for Borehole No.3

Location: Australian Embassy, Maharajganj, Kathmandu

Distance from source to borehole: 3 m

tanθ=L/D, Corrected time (T')=T cosθ

D, m	L, m	θ	cosθ	P-wave		S-wave	
				T, ms	T', ms	T, ms	T', ms
0	3			17.01	0	25.6	0
1	3	71.56	0.3163	14.4	4.55	28	8.86
2	3	56.3	0.5548	14.45	8.02	24.8	13.75
3	3	45	0.7071	9.16	6.47	27.6	19.51
4	3	36.87	0.79999	9.16	7.32	30.5	24.4
5	3	30.96	0.8575	2.61	2.23?	36	30.87
6	3	26.56	0.8944	8.18	7.31	44	39.356
7	3	23.2	0.9191	4.25	3.91	49.6	45.58
8	3	20.55	0.93636	5.2	4.86	53.6	50.18
9	3	18.43	0.94871	10.14	9.61	56	53.12
10	3	16.7	0.9578	12.43	11.9	60	57.46
11	3	15.25	0.96478	7.85	7.57	62.4	60.20
12	3	14.04	0.97012	10.47	10.15	66.4	64.41
13	3	12.99	0.9744	12.43	12.11	70.4	68.59
14	3	12.09	0.97781	13.74	13.43	73.2	71.57
15	3	11.31	0.9805	15.38	15.01	76.4	74.09
16	3	10.62	0.98287	15.38	15.11	80.8	79.41
17	3	10	0.9848	15.38	15.15	85	83.7
18	3	9.46	0.9864	15.05	14.84	87.6	86.4
19	3	8.97	0.9877	16.36	16.15	91.2	90.07
20	3	8.53	0.9889	19.19	18.97	96.4	95.32
21	3	8.13	0.9899	20.28	20.07	98.4	97.40
22	3	7.76	0.9908	22.25	22.04	102	101.06
23	3	7.43	0.9916	27.7	27.46	104.8	103.91
24	3	7.12	0.9922	27.7	27.5	108.4	107.55
25	3	6.84	0.99288	28.79	28.58	111.6	110.8
26	3	6.58	0.9934	24	23.84	114	113.24
27	3	6.34	0.99388	29.78	29.59	116.4	115.68
28	3	6.11	0.9943	31.08	30.9	120.4	119.71
29	3	5.90	0.9947	31.08	30.91	124.8	124.13
30	3	5.71	0.9950				

Note: Measurement was carried out in PVC cased borehole

ANNEX -V

Detail of the calculation of vertical travel time for Borehole No. 5

Location: Australian Embassy, Maharajganj, Kathmandu

Distance from source to borehole: 3 m
tanθ =L/D, Corrected time (T') =T cosθ

D, m	L, m	θ	cosθ	P-wave		S-wave	
				T, ms	T', ms	T, ms	T', ms
0	3			11.35	0	21.6	0
1	3	71.56	0.3163	9.11	2.88	16	5.06
2	3	56.3	0.5548	11.5	6.38	21	11.65
3	3	45	0.7071	13.91	9.83	24.4	17.25
4	3	36.87	0.79999	13	10.4	26.2	20.95
5	3	30.96	0.8575	12.95	11.10	27.6	23.66
6	3	26.56	0.8944	13.11	11.72	33.6	30.05
7	3	23.2	0.9191	14.87	13.66	36	33.08
8	3	20.55	0.93636	17.27	16.17	39.6	37.08
9	3	18.43	0.94871	18.24	17.30	43.8	41.55
10	3	16.7	0.9578	20	19.15	46.6	44.63
11	3	15.25	0.96478	20.96	20.22	49.6	47.85
12	3	14.04	0.97012	21.76	21.11	55	53.35
13	3	12.99	0.9744	22.4	21.82	57	55.54
14	3	12.09	0.97781	22.8	22.29	60.6	59.25
15	3	11.31	0.9805	23.2	22.74	65	63.73
16	3	10.62	0.98287	24.16	23.74	69.2	68.01
17	3	10	0.9848	25.28	24.89	72	70.90
18	3	9.46	0.9864	26	25.64	80	78.91
19	3	8.97	0.9877				
20	3	8.53	0.9889				
21	3	8.13	0.9899				
22	3	7.76	0.9908				
23	3	7.43	0.9916				
24	3	7.12	0.9922				
25	3	6.84	0.99288				
26	3	6.58	0.9934				
27	3	6.34	0.99388				
28	3	6.11	0.9943				
29	3	5.90	0.9947				
30	3	5.71	0.9950				

Note: Measurement was carried out in PVC cased borehole

ANNEX - VI

Detail of the calculation of vertical travel time for Borehole No. 8

Location: Australian Embassy, Maharajganj, Kathmandu

Distance from source to Borehole: 3 m

tanθ=L/D, Corrected time (T')=T cosθ

D, m	L, m	θ	cosθ	P-wave		S-wave	
				T, ms	T', ms	T, ms	T', ms
0	3			11.36	0	20.4	0
1	3	71.56	0.3163	8.5	2.69	10	3.16
2	3	56.3	0.5548	10.24	5.68	23	12.76
3	3	45	0.7071	10.59	7.49	19.2	13.58
4	3	36.87	0.79999	12.4	9.92	22	17.60
5	3	30.96	0.8575	12.9	11.06	26.4	22.64
6	3	26.56	0.8944	14.7	13.15	31.6	28.26
7	3	23.2	0.9191	15.67	14.40	38	34.93
8	3	20.55	0.93636	16.8	15.73	43	40.26
9	3	18.43	0.94871	20.6	19.54	49	46.49
10	3	16.7	0.9578	22	21.07	50	47.89
11	3	15.25	0.96478	22.7	21.90	55.6	53.64
12	3	14.04	0.97012	24.63	23.89	60	58.21
13	3	12.99	0.9744	25.6	24.94	63.2	61.58
14	3	12.09	0.97781	25.75	25.18	66	64.54
15	3	11.31	0.9805	25.9	25.39	70	68.64
16	3	10.62	0.98287	27.2	26.73	73.6	72.34
17	3	10	0.9848	27.5	27.08	76.4	75.24
18	3	9.46	0.9864	25.6	25.25	79.2	78.12
19	3	8.97	0.9877	28.8	28.45	83	81.98
20	3	8.53	0.9889	29.59	29.26	86	85.05
21	3	8.13	0.9899	30.87	30.56	88	87.11
22	3	7.76	0.9908	32.5	32.20	90	89.17
23	3	7.43	0.9916	34.72	34.43	94	93.21
24	3	7.12	0.9922	37.2	36.91	96.4	95.65
25	3	6.84	0.99288	36.32	36.06	99.6	98.89
26	3	6.58	0.9934	36.8	36.56	101.6	100.93
27	3	6.34	0.99388	38	37.77	105	104.36
28	3	6.11	0.9943				
29	3	5.90	0.9947				
30	3	5.71	0.9950				

Note: Measurement was carried out in PVC cased borehole

ANNEX - VII

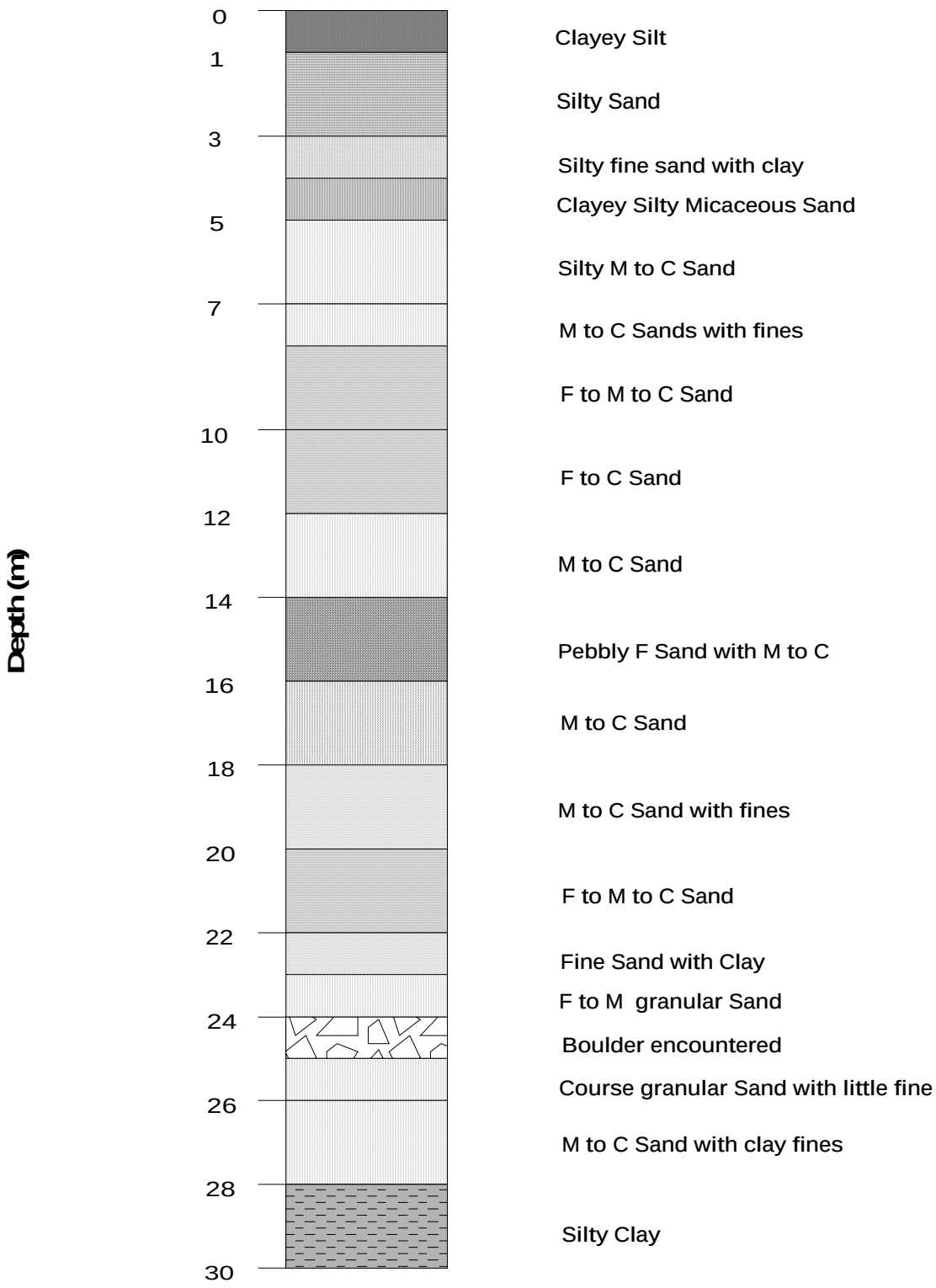

LITHOLOG AT AUSTALIAN EMBASSY FOR BOREHOLE- 3

F – Fine ; M – Medium ; C – Coarse

ANNEX - VIII

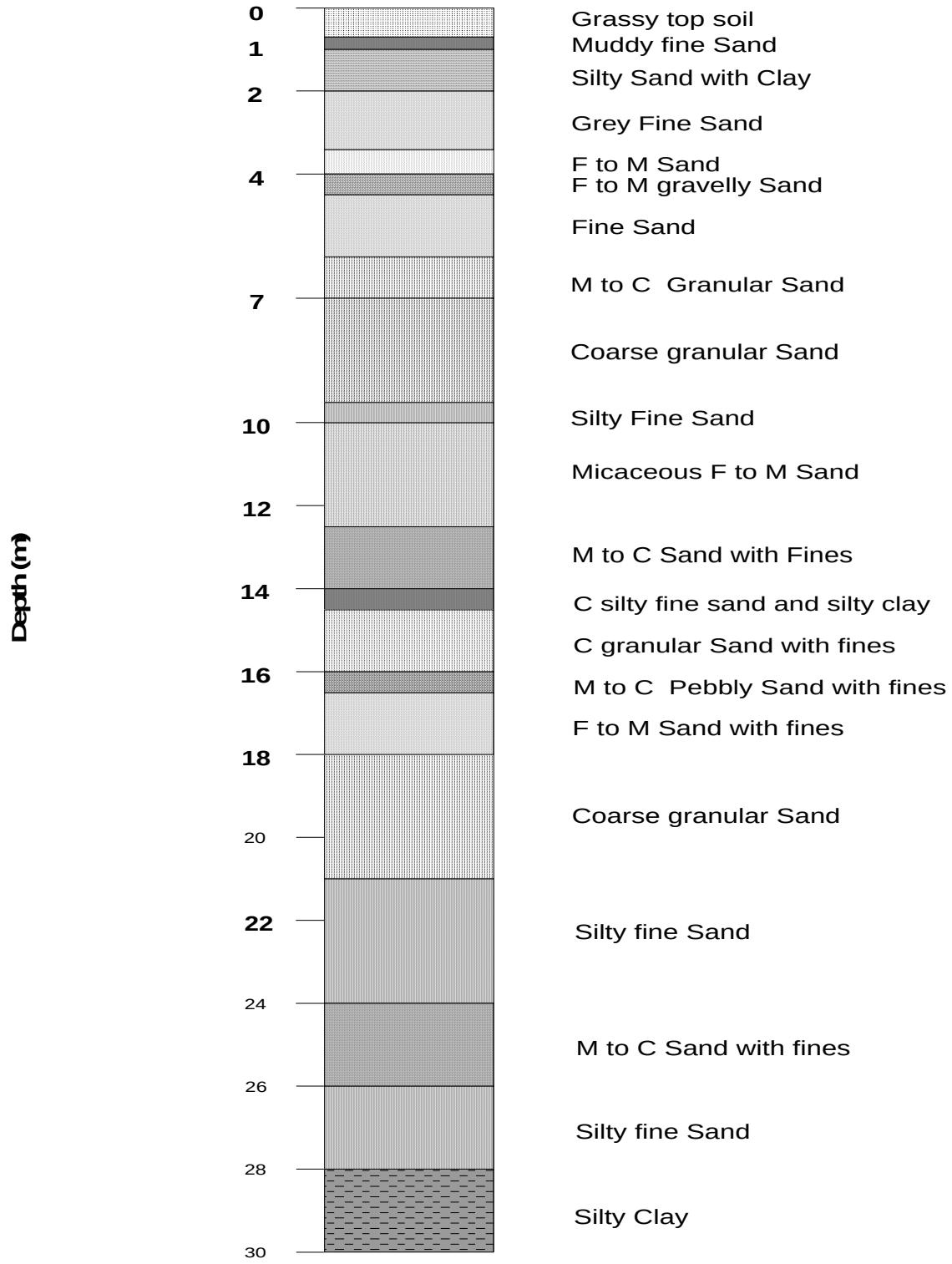

LITHOLOG AT AUSTALIAN EMBASSY FOR BOREHOLE- 5

F – Fine ; M – Medium ; C – Coarse

ANNEX – IX

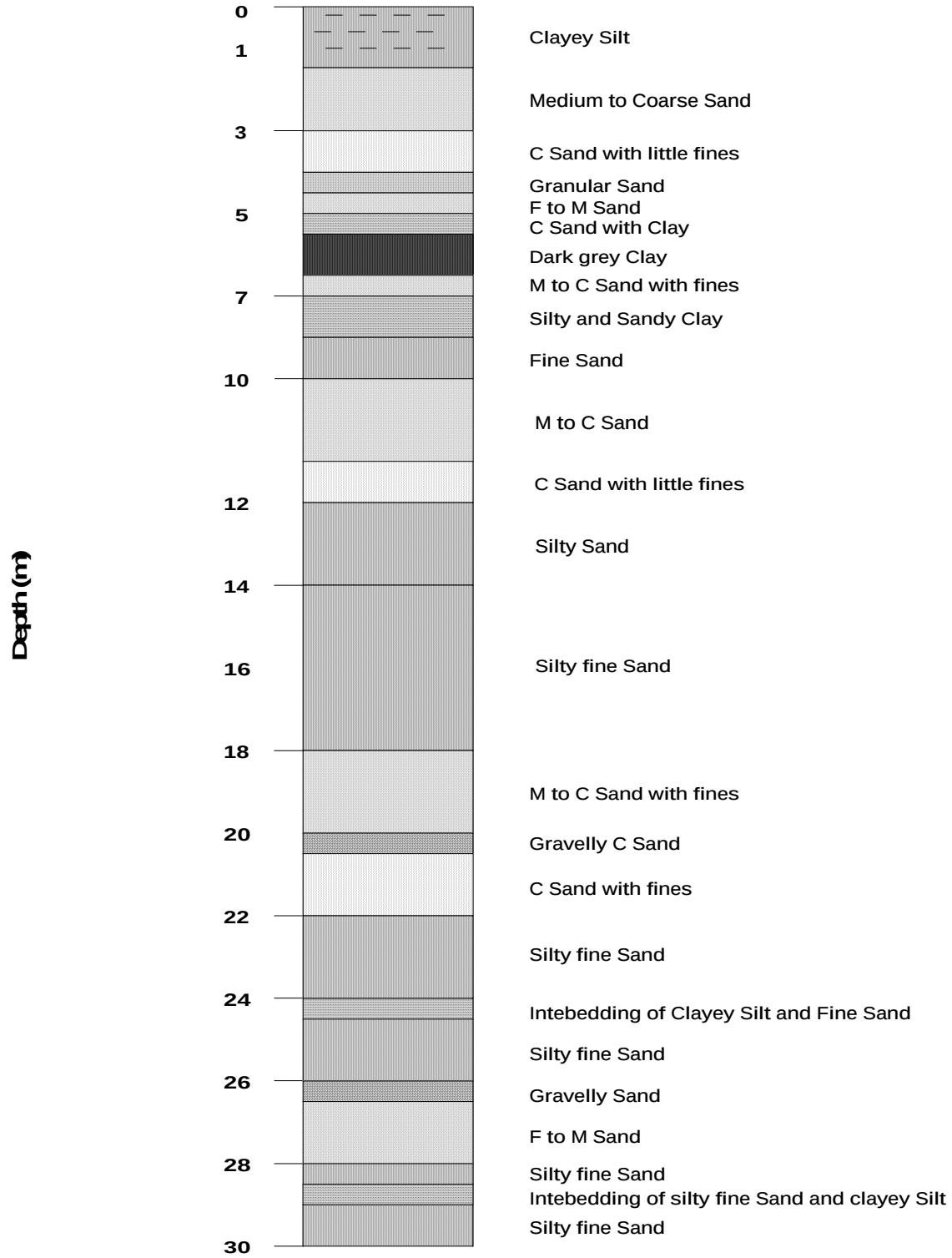

LITHOLOG AT AUSTALIAN EMBASSY FOR BOREHOLE- 8

F – Fine ; M – Medium ; C – Coarse

ANNEX - X

Calculation of effective stress for Borehole -3

$\sigma_v' = \rho_s gh - \rho_w gh$

Where ρ_s = density of soil, ρ_w = density of water, h = thickness of soil layer

σ_v' = effective overburden stress

F = Fine ; M = Medium ; C = Coarse ; bgl = Below ground level

Depth bgl (m)	**Sediment type**	**Thickness (m)**	**Average Density ρ (g/cm^3)**	**g (m/s^2)**	**Stress at 1m (KN/m^2)**	**Over-burden Stress (KN/m^2)**	**Depth from water table (m)**	**Density of water (g/cm^3)**	**Pore pressure (KN/m^2)**	**Effective Stress σ_v' (KN/m^2)**
1	Clayey Silt	1	1.65	9.8	16.17	16.17	0	1	0	16.17
2	Silty sand	1	1.74	9.8	17.052	33.222	0	1	0	33.222
3	Silty sand	1	1.74	9.8	17.052	50.274	1	1	9.8	40.474
4	Silty fine sand with clay	1	1.74	9.8	17.052	67.326	2	1	19.6	47.726
5	Clayey Silty micaceous Sand	1	1.74	9.8	17.052	84.378	3	1	29.4	54.978
7	Silty M. To C. sand	2	1.74	9.8	34.104	118.482	5	1	49	69.482
8	M. to C. sand with fines	1	1.96	9.8	19.208	137.69	6	1	58.8	78.89

9.5	F. To M.to C. sand	1.5	1.96	9.8	28.812	166.502	7.5	1	73.5	93.002
10	F. To M.to C. sand	0.5	1.96	9.8	9.604	176.106	8	1	78.4	97.706
12	F. To C. sand	2	1.96	9.8	38.416	214.522	10	1	98	116.522
14	M. to C. sand	2	1.96	9.8	38.416	252.938	12	1	117.6	135.338
16	Pebbly F. sand with M. To C.	2	1.96	9.8	38.416	291.354	14	1	137.2	154.154
18	M. To C. Sand	2	1.96	9.8	38.416	329.77	16	1	156.8	172.97
20	M. to C. sand with fines	2	1.96	9.8	38.416	368.186	18	1	176.4	191.786
22		2	1.96	9.8	38.416	406.602	20	1	196	210.602
26		4	2	9.8	78.4	485.002	24	1	235.2	249.802
30		4	2	9.8	78.4	563.402	28	1	274.4	289.002

ANNEX - XI

Calculation of effective stress for Borehole -5

$\sigma_v' = \rho_s gh - \rho_w gh$

Where ρ_s = density of soil, ρ_w = density of water, h = thickness of soil layer

σ_v' = effective overburden stress

F = Fine ; M = Medium ; C = Coarse ; bgl = Below ground level

Depth bgl (m)	**Sediment type**	**Thickness (m)**	**Average Density ρ (g/cm^3)**	**g (m/s^2)**	**Stress at 1m (KN/m^2)**	**Over-burden Stress (KN/m^2)**	**Depth from water table (m)**	**Density of water (g/cm^3)**	**Pore pressure (KN/m^2)**	**Effective Stress σ_v' (KN/m^2)**
1	Muddy fine Sand	1	1.7	9.8	16.66	16.66	0	1	0	16.66
2	Fine Sand with Clayey Silt	1	1.7	9.8	16.66	33.32	0	1	0	33.32
3	Fine Sand	1	1.7	9.8	16.66	49.98	0	1	0	49.98
4	F. to M. Sand	1	1.85	9.8	18.13	68.11	0.2	1	1.96	66.15
4.5	F. To M. Gravelly Sand	0.5	1.85	9.8	9.065	77.175	0.7	1	6.86	70.315
6	Fine Sand	1.5	1.85	9.8	27.195	104.37	2.2	1	21.56	82.81

7	M. To C. Sand with fines	1	2	9.8	19.6	123.97	3.2	1	31.36	92.61
8	Coarse granular Sand	1	2	9.8	19.6	143.57	4.2	1	41.16	102.41
9	C. Ganular Sand with fines	1	2	9.8	19.6	163.17	5.2	1	50.96	112.21
10	C. To silty F. Sand	1	2	9.8	19.6	182.77	6.2	1	60.76	122.01
12	Silty F. Sand	2	2	9.8	39.2	221.97	8.2	1	80.36	141.61
14	M. To C. Sand with fines	2	2	9.8	39.2	261.17	10.2	1	99.96	161.21
16	C. Granular Sand with fines	2	2	9.8	39.2	300.37	12.2	1	119.56	180.81
18	M. To C. Pebbly Sand with fines	2	2	9.8	39.2	339.57	14.2	1	139.16	200.41
20	C. Granular Sand	2	2	9.8	39.2	378.77	16.2	1	158.76	220.01
22		2	2	9.8	39.2	417.97	18.2	1	178.36	239.61
24		2	2	9.8	39.2	457.17	20.2	1	197.96	259.21
26		2	2	9.8	39.2	496.37	22.2	1	217.56	278.81
28		2	2	9.8	39.2	535.57	24.2	1	237.16	298.41

ANNEX - XII

Calculation of effective stress for Borehole -8

$\sigma_v' = \rho_s gh - \rho_w gh$

Where ρ_s = density of soil, ρ_w = density of water, h = thickness of soil layer

σ_v' = effective overburden stress

F = Fine ; M = Medium ; C = Coarse ; bgl = Below ground level

Depth bgl (m)	**Sediment type**	**Thickness (m)**	**Average Density ρ (g/cm^3)**	**g (m/s^2)**	**Stress at 1m (KN/m^2)**	**Over-burden Stress (KN/m^2)**	**Depth from water table (m)**	**Density of water (g/cm^3)**	**Pore pressure (KN/m^2)**	**Effective Stress σ_v' (KN/m^2)**
1	Clayey Silt	1	1.9	9.8	18.62	18.62	0	1	0	18.62
2	F. To C. Sand with Clayey Silt	1	1.9	9.8	18.62	37.24	0	1	0	37.24
3	M. To C. Sand	1	1.9	9.8	18.62	55.86	0	1	0	55.86
4	C. Sand with little fines	1	1.9	9.8	18.62	74.48	0.8	1	7.84	66.64
5	F. To M. Granular Sand	1	1.86	9.8	18.228	92.708	1.8	1	17.64	75.068
6	C. Sand with Clay	1	1.86	9.8	18.228	110.936	2.8	1	27.44	83.496
7	Clay with M. To C. Sand	1	1.86	9.8	18.228	129.164	3.8	1	37.24	91.924

8	Silty to Sandy Clay	1	1.86	9.8	18.228	147.392	4.8	1	47.04	100.352
9	Fine Sand	1	1.97	9.8	19.306	166.698	5.8	1	56.84	109.858
10	M. To C. Sand	1	1.97	9.8	19.306	186.004	6.8	1	66.64	119.364
12	M. To C. granular Sand	2	1.97	9.8	38.612	224.616	8.8	1	86.24	138.376
14	Silty F. To M. to C. Sand	2	1.96	9.8	38.416	263.032	10.8	1	105.84	157.192
16	Silty F. Sand	2	1.96	9.8	38.416	301.448	12.8	1	125.44	176.008
18	Silty F. Sand	2	1.96	9.8	38.416	339.864	14.8	1	145.04	194.824
20	M. To C. Sand with fines	2	1.96	9.8	38.416	378.28	16.8	1	164.64	213.64
22		2	1.96	9.8	38.416	416.696	18.8	1	184.24	232.456
24		2	2.01	9.8	39.396	456.092	20.8	1	203.84	252.252
26		2	2.01	9.8	39.396	495.488	22.8	1	223.44	272.048
28		2	2.01	9.8	39.396	534.884	24.8	1	243.04	291.844

ANNEX – XIII

Source Zone	EQ Sources	Fault Name	Fault Type	Hypocentral distance (km)	Assumed M max
1	HFF - 1.10	Narayani river	R/RL	84.12	6.7
2	HFF - 1.15	Dhalkebar	R/RL	110.58	7.2
3	MBT - 2.3	Arung Khola	R- N down	172.18	7.5
4	MBT -2.4	Narayani river	R	81.97	7
5	MBT - 2.5	Hetauda	R	41.18	7.3
6	MCT - 3.3	Gosainkunda	R	20	7.6
7	HFT -1.13	Amlekhgunj	R	52.35	7
8	LH - 4.7	Saptakoshi -Deomai	R	69.42	7
9	MBT - 2.6	Udaipur - Sunkoshi	R-N	140.12	8
10	LH -2.7	Saptakoshi -Deomai	R	222.2	7.5

Earthquake sources and their hypocentral distance (Adapted from Chaudhary, A.K. 2007, M.Sc. Dissertation, Tribhuvan University)

ANNEX – XIV

Borehole - 3				Borehole - 5				Borehole - 8			
Depth	**Field spt N**	**N_c**	**$(N_1)_c$**	**Depth**	**Field spt N**	**N_c**	**$(N_1)_c$**	**Depth**	**Field spt N**	**N_c**	**$(N_1)_c$**
1	3	3	7	1	4	4	10	2	18	17	38
2	11	11	19	2	4	4	7	3	21	18	29
3	13	13	20	3	6	6	8	4	15	15	20
4	5	5	7	4	5	5	6	5	9	9	11
5	7	7	9	5	12	12	14	6	36	26	29
7	58	37	44	6	26	21	23	7	9	9	10
8	36	26	29	7	25	20	21	8	51	33	34
10	35	25	26	8	51	33	33	9	19	17	17
10	35	25	25	9	24	20	18	10	33	24	23
12	36	26	24	10	31	23	21	12	23	19	17
14	22	19	16	12	33	24	20	14	36	26	22
16	38	27	21	14	32	24	19	16	51	33	26
18	43	29	22	16	64	40	29	18	62	39	29
20	78	47	34	18	78	47	33	20	58	37	26
22	34	25	17	20	63	39	26	22	69	42	29
26	53	34	22	22	82	49	31	24	60	38	25
30	58	37	21	24	110	63	39	26	83	49	31
				26	62	39	23	28	76	46	28
				28	32	24	14				

Correction of SPT data